

# Modelling the interaction between the atmosphere and curing concrete bridge decks with the SLABS model

Gary S Wojcik<sup>1</sup>, David R Fitzjarrald<sup>1</sup> & Joel L Plawsky<sup>2</sup>

<sup>1</sup>Atmospheric Sciences Research Center, University at Albany, State University of New York, 251 Fuller Road, Albany, NY 12203-3649

<sup>2</sup>Department of Chemical Engineering, Rensselaer Polytechnic Institute, Troy, NY 12180-3590  
email: gwojcik@nist.gov

---

*The interaction between atmospheric and construction conditions and the exothermic, temperature-dependent hydration reactions of the concrete's binding components may produce adverse conditions in curing concrete, thereby reducing the quality of that concrete. Accurate model forecasts of concrete temperatures and moisture would help engineers determine an optimal time to pour, an optimal mix design, and/or optimal curing practices. Existing models of curing concrete bridge decks and road surface prediction models lack realistic boundary conditions. The concrete models contain unnecessarily detailed hydration heat generation mechanisms for a simplified field forecast model. In this paper, a new energy balance model (SLABS), which can be easily adapted to predict road surface conditions, is described and applied to predict the temperatures and moisture of curing concrete bridge decks made with New York State Department of Transportation's Class HP concrete. Highest concrete temperatures occurred at high air temperatures, humidities and initial concrete temperatures and at low cloud cover fractions and wind speeds. Peak concrete temperatures can exceed 60 °C. To minimise concrete temperatures and temperature gradient magnitudes, concrete should be placed during the late afternoon or early evening. As a field forecast model for which the meteorological inputs are taken from NGM MOS forecasts, the outputs of SLABS include the peak concrete temperature (to within 2 °C of the observed in one application), peak temperature gradient, evaporation rate at the time of placement and several warning messages indicating adverse field conditions.*

## 1. Introduction

The internal and surface temperatures of concrete bridge decks are determined mainly by local surface energy fluxes, starting roughly a day after the concrete is placed (the passive state). During the first day or so after placement, however, the temperatures are determined by the interaction between the local energy fluxes and temperature-dependent, exothermic hydration reactions of the concrete's binder components (the active state). This interaction can lead to increases in concrete temperatures of up to 40 °C in the case of bridge decks.

The long-term durability and strength of a concrete mass may be compromised by excessive concrete temperatures and temperature gradients or insufficient moisture during the first few days after the concrete is placed, when the concrete is 'cured' (FitzGibbon 1976a, 1976b; Gopalan and Haque 1987; Neville 1996: 359–411). Such detrimental concrete conditions may be caused by adverse construction practices (concrete mix

design, curing procedures, initial concrete temperatures, time of placement) or adverse atmospheric conditions. Accurate model forecasts of concrete temperatures and moisture would help engineers determine an optimal time to pour, an optimal mix design including the initial concrete temperature, or optimal curing practices. Previous modelling studies of the interaction between atmospheric and construction conditions and curing concrete have not used proper boundary conditions and so there is a need for a modelling study to determine the extent of this interaction on concrete temperatures and quality (Wojcik & Fitzjarrald 2001). Such a modelling system requires accurate treatment of both the internal heat source and the boundary conditions. In this paper, we present a new one-dimensional energy balance model (SLABS: SUNY Local Atmosphere Bridge Simulation) applied to determine the sensitivity of curing concrete bridge temperatures and moisture to atmospheric and construction conditions. SLABS can be easily adapted to predict the state of road surfaces and addresses some limitations in existing road model systems.

### 1.1. Energy balances of curing concrete bridge decks

Like most surfaces, bridge decks and roads experience sensible, latent, radiative and ground heat fluxes (Figure 1a). For bridge decks, the bottom surface heat transfer from net radiation and sensible heat must also be considered. The energy balance for a concrete bridge deck in its active state also includes the internal hydration heat source from the concrete's binding components (cement, microsilica, and flyash for Class HP concrete used by the New York State Department of Transportation (NYSDOT 1999), a variation of Class H concrete binder which contains cement and flyash). Excess water from irrigation hoses is sprayed on the curing deck's top surface (covered with burlap) for several days to facilitate the top surface hydration reactions and to remove heat.

The hydration reactions consist of four stages, each distinct in their heat generation rates (Figure 1b). Upon mixing with water, surface reactions produce a 'gel' on cementitious particles and release heat (Stage I). The presence of the gel impedes the diffusion of water into the cement particle slowing the hydration for several hours (Stage II). When the water reaches the unhydrated cement, vigorous hydration and heat development occurs lasting up to 24 h (Stage III; setting occurs at the beginning of Stage III). After Stage III, the hydration reactions diminish considerably but will continue for many years (Stage IV). The deck is essentially a passive volume during Stage IV. Stage II can be extended by the addition of small amounts of retarders, generally in liquid form, into the concrete mix. The use of retarders is often necessary for large pours of concrete where the setting of one area before another could lead to cracking. By increasing the length of Stage II with retarders, this problem can be avoided. For more details of cement and concrete chemistry, see Neville (1996), Taylor (1997), Wojcik et al. (2001) and Wojcik (2001).

The first estimates of the magnitudes of heat transfer mechanisms for curing bridges were determined by Wojcik and Fitzjarrald (2001) for four bridges in eastern and central New York in 1995, 1996, 1998 and 1999. They found that the magnitude of each transfer term varied according to the atmospheric conditions, suggesting that concrete conditions will vary depending on season, location and time of placement. Between 70 and 85% of the heat transfer occurred at the top surface and most was transferred by evaporation or the runoff water, with the evaporation dominating when wind speeds were  $>1 \text{ m s}^{-1}$ . The total amount of heat that was lost through the top surface at night during Stage III was up to three times greater ( $360 \text{ W m}^{-2}$  compared with  $120 \text{ W m}^{-2}$ ) than that when the bridge was no longer generating significant heat (Stage IV), indicating the vigour of the hydration reactions. Steel beams supporting the concrete from below (Figure 1a)

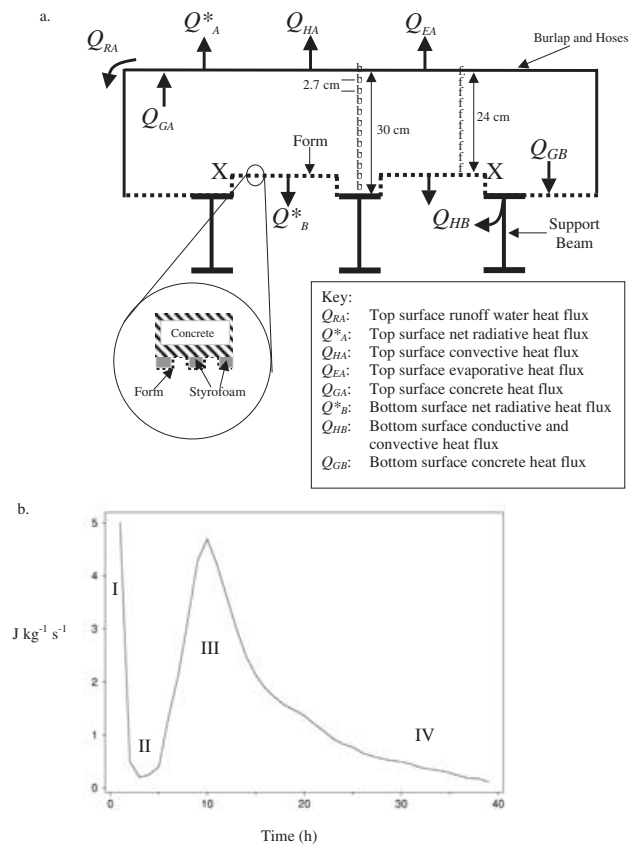


**Figure 1.** (a) Schematic cross-section of a bridge deck indicating the energy balance terms used as boundary conditions in the SLABS model. Not to scale. The concrete thickness averaged about 29 cm and the minimum width of the bridges studied was 9.8 m. The arrows indicate the typical direction of energy flow when the peak concrete temperatures occur during the night; 'b' and 'f' indicate grid points above a beam and the form, respectively. (b) A typical example of heat generation rates ( $\text{J kg}^{-1} \text{ s}^{-1}$ ) for hydrating cement. Roman numerals indicate the stages in the hydration process.

also transferred significant heat, but this heat transfer was limited to the regions directly above the beams, or ~20% of the bottom surface area of the bridge decks.

### 1.2. Boundary condition validation in road model systems

Some road models employ surface energy balance techniques to predict the road surface temperatures and road moisture type and amount (e.g. Rayer 1987; Sass 1997; Crevier & Delage 2001). Other road models also use statistical techniques with current and historical data (e.g. Shao & Lister 1996; Jacobs 1997). While predictions of road surface temperatures by the energy balance models are within  $2^\circ\text{C}$  of the observed values at many times, their validation procedures and the model flux parameterisations have limitations. For example, these models use surface layer similarity hypotheses and assumed roughness lengths to compute exchange coefficients for convective fluxes in road environments. These road environments do not represent homogeneous conditions, as this type of similarity

requires (e.g. Chen et al. 1999). Another limitation is that only the surface temperature predictions and not the surface flux predictions are verified. Radiation is the dominant term in the surface energy balance (e.g. Wojcik & Fitzjarrald 2001). Some radiation parameterisations in these models are highly detailed, including information about aerosols, ozone and shading effects (Rayer 1987; Sass 1997; Crevier & Delage 2001). However, no radiation measurements are made at typical roadside weather stations and we have found no comparisons of observed and predicted values of any of the road surface flux terms. Furthermore, systematic biases in temperature predictions are sometimes arbitrarily fixed by applying a correction factor to the radiation terms until the observed and predicted temperatures match (e.g. Crevier & Delage 2001).

### 1.3. Current concrete placement and curing specifications

To attain its maximum service life and durability, concrete should develop low permeability and porosity to reduce the ingress of water, road chemicals and other pollution. Placement and curing specifications are implemented so that such properties develop by ensuring that:

- the concrete temperatures and temperature gradients do not become too large,
- the concrete doesn't freeze, which would limit hydration and produce cracking due to the expansion of freezing water, and
- the concrete top surface remains moist.

These factors, as well as temperature and stress development during the first several hours of hydration, the rigidity of the mass during the cooling phase of the hydration, and the degree of structural restraint, will determine the concrete quality (Emborg 1990; Roelfstra et al. 1994; Mangold & Springenschmid 1994). The stresses, restraints and rigidity of the concrete mass are beyond the scope of the present study and we focus on the concrete temperatures.

While moist curing for a period of several days or more is widely used for bridge decks, there is no consensus

about other curing and placement conditions (Table 1). For example, NYSDOT states that the air temperature at the time of placement and during curing should not be below 7 °C (NYSDOT 1998), while the Minnesota Department of Transportation (MNDOT) declares that it should not be below 2 °C (MNDOT 2002). The MNDOT specifications also state that as long as moist curing is applied, normal air temperatures in spring, summer and fall are not detrimental to the concrete. The American Concrete Institute (ACI), however, reports that the concrete quality may suffer under high ambient air temperatures (ACI 1991). Because conditions and materials vary widely, the ACI asserts that it is impractical to recommend a limiting air or concrete temperature above which the quality of the concrete will be greatly diminished. Finally, the ACI suggests that the evaporation rate during the placement should not exceed 680 W m<sup>-2</sup> (ACI 1991), while the NYSDOT states that it should not be above 830 W m<sup>-2</sup> (NYSDOT 1998). We note that, in practice, ensuring good curing can be very difficult on site due to construction schedules, environment issues and construction features.

A field engineer who must follow such specifications, among other duties, is responsible for determining the best time for the concrete to be placed, the best curing procedures, and the best mix design so that the concrete can attain its best possible strength and durability while keeping construction costs within budgetary limits. The NYSDOT and MNDOT specifications are based on studies that had unrealistic boundary conditions and so may be of little use to engineers. Furthermore, because the interaction between the heat and water transfer and the hydration reactions determines the thermal and moisture states of the curing concrete, the concrete conditions will vary depending on the season and location. Therefore, the application of such specifications to all freshly placed concrete is dubious, emphasising the need for an operational field forecast model to determine the best time to pour, the best mix design, or the best curing practices based on predicted concrete conditions.

We have developed the SLABS model to study the sensitivity of concrete temperatures and moisture to atmospheric and construction conditions and to comment on the practicality of current placement and

Table 1. *Current concrete placement and curing specifications for several agencies.*

Specification	NYSDOT	MNDOT	ACI
Initial Concrete Temperature	—	10–32 °C	—
Evaporation Rate at Placement	≤830 W m <sup>-2</sup>	—	≤680 W m <sup>-2</sup>
Air Temperature at Placement and during Curing	≥7 °C	≥2 °C	≤24–38 °C
Curing Method	Moist Curing with burlap for 14 days (burlap placed within 30 minutes of concrete placement)	Moist Curing with burlap	Moist Curing with burlap
Concrete Cooling Rate	—	—	3 °C h <sup>-1</sup> or 28 °C day <sup>-1</sup>

curing specifications. In the process, we have validated our model boundary conditions with both estimated and measured bridge temperatures and fluxes, addressing a limitation of previous road modelling studies. The model is simple enough to allow a field engineer to make appropriate on-site decisions based on weather forecasts, and is flexible enough to accurately account for the heat and mass transfer that occurs in any atmospheric conditions.

In the following, we provide a description of the SLABS model in section 2, which also includes a discussion of the boundary conditions and the heat generation formulation. In section 3, we evaluate the model boundary condition parameterisations and the model's sensitivities to various physical and chemistry parameters. We also present in section 3 an analysis of the sensitivity of the model predictions of concrete temperatures, binder concentrations and water concentrations to: (i) many atmospheric conditions including those in various climates and seasons; and (ii) construction practices such as the time of placement and the initial concrete temperature. In section 3, we also comment on current curing and placement specifications and apply the model as an operational forecast model to one of the bridges studied in our field work. This work is summarised in section 4.

## 2. Methodology

In a typical bridge that we studied (Wojcik & Fitzjarrald 2001), the concrete had different thicknesses depending on the given horizontal location (Figure 1a). The concrete is ~6 cm thicker over the steel support 'I' beams (30 cm) than it is over the 'form' (a thin, shiny, corrugated, galvanised steel sheet supporting the concrete from below) (24 cm). The steel beams and half of the steel form are in direct contact with the concrete. The other half of the steel form is covered by styrofoam to reduce the amount of concrete that is used. At the top surface, the concrete was covered with burlap and sprayed with water from irrigation hoses for up to 14 days after placement.

### 2.1. SLABS model

The SLABS model is a 1D finite difference model which solves the governing equations by using a fully implicit Crank-Nicolson scheme for the diffusion of heat and moisture (Press et al. 1992: 637–640) and a fourth-order Runge-Kutta scheme for the chemistry (Press et al. 1992: 550–554). For simulations of locations at or above the form, the SLABS model consists of ten vertical grid points (nine layers) with a grid size of 2.7 cm and predicts the vertical temperatures and water and binder concentrations in the concrete slab (Figure 1a). When applied over the beams, the model

consists of 12 vertical grid points (11 layers). Each grid point corresponds to a point at which the NYSDOT took vertical concrete temperature measurements. The governing equations are:

Binder concentration,  $B$  ( $\text{mol}_B \text{ m}_{\text{con}}^{-3}$  (con=concrete)):

$$\frac{dB}{dt} = -k \cdot B^n \cdot R^m \quad (1)$$

where  $R$  ( $\text{mol}_R \text{ m}_{\text{con}}^{-3}$ ) is the concentration of water available for the hydration reactions;  $n$  and  $m$  are exponents whose sum gives the order of the hydration reaction ( $n=m=1$ );  $k$  ( $\text{m}_{\text{con}}^3 \text{ mol}_R^{-1} \text{ s}^{-1}$ ) is the reaction rate constant given by:

$$k = A \cdot \exp\left(-\frac{Ea}{R^* \cdot T_c}\right) \quad (2)$$

where  $Ea$  is the activation energy,  $A$  is the pre-exponential factor;  $R^*$  is the universal gas constant ( $8.314 \text{ J mol}^{-1} \text{ K}^{-1}$ ), and  $T_c$  (K) is the concrete temperature. Wojcik et al. (2001) provided justification for  $n=m=1$ , determined that  $Ea=35 \text{ kJ mol}^{-1}$  and found  $A=0.0015-0.0033$  for simple calorimetry experiments.

Concrete temperature,  $T_c$ :

$$\frac{dT_c}{dt} = K_T \frac{\partial^2 T_c}{\partial z^2} - V \cdot \frac{dB}{dt} \quad (3)$$

where the second term on the right hand side of Eq. (3) is the hydration heat source term where  $V$  ( $\text{K m}_{\text{con}}^3 \text{ mol}_B^{-1} \text{ s}$ ) converts the reacted binder concentration to heat and is equal to  $-\Delta H^* M_{wB} / \rho_c c_{pc}$ ;  $-\Delta H^*$ : the hydration heat of Class HP concrete ( $\sim 420 \text{ kJ kg}_{\text{binder}}^{-1}$ );  $c_{pc}$ : the specific heat of Class HP concrete ( $\sim 1380 \text{ J kg}^{-1} \text{ K}^{-1}$ ); and  $\rho_c$ : the density of Class HP concrete ( $\sim 2230 \text{ kg m}_{\text{con}}^{-3}$ ).  $K_T$  is the thermal diffusivity of concrete ( $\sim 8.8 \times 10^{-7} \text{ m}_{\text{con}}^2 \text{ s}^{-1}$ ), determined from  $\rho_c$ ,  $c_{pc}$ , and the Class HP thermal conductivity,  $k_c$  ( $\sim 2.7 \text{ W m}^{-1} \text{ K}^{-1}$ ).  $-\Delta H$  was determined with calorimetry experiments and  $\rho_c$  and  $c_{pc}$  were calculated from a concrete sample taken from the batch used at the 1999 bridge (Wojcik & Fitzjarrald 2001; Wojcik et al. 2001). Wojcik & Fitzjarrald (2001) determined  $k_c$  from a heat flux plate and thermocouples placed within the concrete and with the SLABS model.  $M_{wB}$  is the molecular weight of the binder ( $0.191 \text{ kg mol}^{-1}$ ) determined from a mass average weighting of the molecular weights of cement ( $0.232 \text{ kg mol}^{-1}$ ), flyash ( $0.077 \text{ kg mol}^{-1}$ ), and microsilica ( $0.062 \text{ kg mol}^{-1}$ ) (Watt & Thorne 1965; Hjorth 1982; Bureau of Reclamation 1988).

Available water concentration,  $R$  ( $\text{mol}_R \text{ m}^{-3}$ ):

$$\frac{dR}{dt} = K_R \frac{\partial^2 R}{\partial z^2} + \eta \cdot \frac{dB}{dt} \quad (4)$$

where  $K_R$  ( $\sim 10^{-9} \text{ m}^2 \text{ s}^{-1}$ ) is the diffusivity of water in concrete (Pommershiem & Clifton 1991).  $R$  is the water concentration in the concrete that is available for the hydration reactions. We reduce  $K_R$  by a factor of 20 (Powers 1958) when the binder hydration fraction

reaches 0.6. At this hydration fraction, the larger pores in the concrete become segmented (Bentz & Garboczi 1991), significantly limiting the movement of water.

The term  $\eta$  in Eq. (4) represents the number of moles of water removed from the available pool per mole of binder that hydrates. Some water is chemically converted into the hydration products and some is adsorbed onto the surface of the hydration products where it cannot be used for further hydration (Powers & Brownyard 1946–7). Both sinks are taken into account in  $\eta$ . To determine  $\eta$  and  $A$  in Eq. (3), we minimised the temperature root mean square error,  $RMSE$ , for the 1999 bridge by varying  $\eta$  and  $A$  over wide ranges. We determined  $A=0.0039$  and  $\eta=8.3$ . See also section 3.3 for more details on this procedure.

At both the top and bottom surfaces of the bridge deck, the boundary conditions are implemented in flux-conservative form (e.g. Press et al. 1992: 825–838). Such a format is chosen to maintain the stability of the solutions by keeping the second-order accuracy of the implicit Crank-Nicolson scheme. By convention, upward fluxes are positive.

For the top surface, the energy balance ( $W\ m^{-2}$ ) is given by:

$$-Q^*_A + Q_{GA} = Q_{HA} + Q_{EA} + Q_{RA} \quad (5)$$

where  $Q^*_A$  is the net radiation;  $Q_{GA}$  is the heat flux through the concrete top surface;  $Q_{HA}$  is the sensible heat flux;  $Q_{EA}$  is the heat flux due to the evaporation of water; and  $Q_{RA}$  is the runoff water heat flux (Figure 1a).

The top surface energy flux ( $Q_{GA}$ ) is given by:

$$Q_{GA} = -k_c \frac{dT_c}{dz} = \quad (6)$$

$$-Q^*_A - \rho L_v C_e U (q_a - q_s) - \rho c_p C_b U (T_a - T_s) - \rho_w c_w (T_{wi} - T_{wf}) \frac{M}{A_{top}}$$

The second term on the right hand side of Eq. (6) is the latent heat flux, the third is the sensible heat flux, and the fourth is the runoff water heat flux.  $M$  represents the volume flow rate of water running off the bridge ( $m^3\ s^{-1}$ );  $A_{top}$  is the area of the bridge's top surface ( $m^2$ );  $q_a$  and  $q_s$  are the air and surface specific humidities ( $g\ g^{-1}$ );  $T_a$  and  $T_s$  are the air and surface temperatures ( $^{\circ}C$ );  $\rho_w$  and  $\rho$  are the water and air densities ( $kg\ m^{-3}$ );  $c_w$  and  $c_p$  are the water and air specific heat capacities ( $J\ kg^{-1}\ K^{-1}$ );  $L_v$  is the latent heat of evaporation ( $J\ kg^{-1}$ );  $U$  is wind speed ( $m\ s^{-1}$ );  $C_e$  and  $C_b$  are dimensionless exchange coefficients;  $z$  is the vertical dimension (m); and  $T_{wi}$  and  $T_{wf}$  are the initial (when hitting the top surface) and final (when running off the bridge) spray water temperatures ( $^{\circ}C$ )

The exchange coefficients,  $C_e=C_b$ , for conditions other than free convection (free convection assumed when the bulk Richardson number,  $Rb$ ,  $< -1$  and  $U < 1\ m\ s^{-1}$ ) were determined by Wojcik & Fitzjarrald (2001) from field measurements and subsequent development of the energy balances of the four curing concrete bridges. Free convection exchange speeds (equal to  $CU$  in Eq. 6) are given by the parameterisation of Kondo & Ishida (1997) for a smooth surface.

The net radiation, the dominant term in the top surface energy balance (Wojcik & Fitzjarrald 2001), is computed in the model by determining the incoming and outgoing longwave and shortwave radiation components. The clear sky, incoming shortwave radiation at the surface ( $K_I$ ) was calculated with a scheme given by Stull (1988: 257–258). The effect of cloud cover fraction,  $clf$ , on  $K_I$  is given by Freedman et al. (2001) as:

$$K_I = 0.91 - (0.7 \cdot clf) \quad (7)$$

The outgoing shortwave radiation,  $K_O$ , is equal to  $0.14 \cdot K_I$ , where 0.14 is the albedo of concrete covered with burlap and sprayed with water (Wojcik & Fitzjarrald 2001).

The clear sky incoming longwave radiation ( $L_I$ ) is given by Stefan-Boltzman's law. The atmospheric emissivity for clear skies,  $\epsilon_{clear}$ , as a function of atmospheric water vapour pressure ( $e_a$ ) and air temperature ( $T_a$ ), is determined with a scheme proposed by Prata (1996):

$$\epsilon_{clear} = 1 - \left( 1 + 46.5 \cdot \frac{e_a}{T_a} \right) \cdot \exp \left\{ - \left( 1.2 + 3 \cdot 46.5 \cdot \frac{e_a}{T_a} \right)^{\frac{1}{2}} \right\} \quad (8)$$

For cloudy skies, the atmospheric emissivity, as a function of vapour pressure, temperature, and  $clf$  is given by Brutsaert (1975):

$$\epsilon_{cloudy} = clf + 1.24 \cdot (1 - clf) \cdot \left( \frac{e_a}{T_a} \right)^{\frac{1}{7}} \quad (9)$$

The outgoing longwave radiation ( $L_O$ ) is given by Stefan-Boltzman's law with a surface emissivity of 0.98 for the wet surfaces of the bridges. Wojcik & Fitzjarrald (2001) determined that these parameterisations generally predict  $Q^*_A$  within  $\pm 60\ W\ m^{-2}$ , although the predictions may be as much as  $100\ W\ m^{-2}$  (15%) too high during the mid-afternoon on sunny days.

The temperature of spray water as it hits the top surface ( $T_{wi}$ ) is determined by assuming the drop temperatures adjust to the environmental conditions as they rise and fall after being ejected from irrigation hoses (Wojcik & Fitzjarrald 2001), as given by a model by Pruppacher & Klett (1997). The drops generally do not remain airborne long enough to approach the air wet-bulb temperature. By assuming they do can result in errors in

$Q_{RA}$  of more than 25% (Wojcik & Fitzjarrald 2001). The runoff water temperature ( $T_{wf}$ ) was assumed to be the top surface concrete temperature, as suggested by Wojcik & Fitzjarrald (2001). When the effects of spray water are simulated, we assume that there is a puddle of water on the top surface ( $R=55555 \text{ mol}_R \text{ m}_R^{-3}$ ) for the top surface water boundary condition.

At the form, the heat flux at the bridge bottom,  $Q_{GB}$  ( $\text{W m}^{-2}$ ), is given by:

$$Q_{GB} = -k_c \frac{dT_c}{dz} = Q_B^* + \rho c_p U C_b (T_a - T_{cf}) \quad (10)$$

where the second term on the right-hand side accounts for convective heat loss;  $T_{cf}$  is the temperature of the form;  $Q_B^*$  is the net radiation at the bottom surface; and  $C_b$  is the exchange coefficient for the form. The layer of air between the beams had a stable stratification (warmest air near the form) and so convective heat loss from the form was small (Wojcik & Fitzjarrald 2001). As such,  $C_b$  is set to  $10^{-5}$  in the model.  $Q_B^*$  at the form was computed by applying Stefan-Boltzman's law to the surface below the bridge and the form for the upward and downward longwave fluxes with the form emissivity of 0.1 and the ground emissivity of 0.98 (water/soil). The net radiation at the form is generally  $25 \text{ W m}^{-2} < Q_B^* < -25 \text{ W m}^{-2}$  much of the time (Wojcik & Fitzjarrald 2001).

Heat transfer through the top of the steel support beams (Figure 1a) is modelled as heat flow through an infinite steel fin (Incropera & DeWitt, 1996, pp. 118). The beam heat loss ( $= Q_{GB}$  when considering just the beam),  $F_{beam}$  ( $\text{W m}^{-2}$ ), is given by:

$$F_{beam} = -\frac{(T_{cs} - T_a) \cdot (bPk_s A_{cf})^{\frac{1}{2}}}{A_{tb}} \quad (11)$$

where  $b$  is the heat transfer coefficient for free convection from a vertical flat plate (Incropera and DeWitt 1996: 457);  $P$  is the perimeter of the fin;  $A_{cf}$  is the cross-sectional area of the fin;  $A_{tb}$  is the surface area of the beam in contact with the concrete;  $T_{cs}$  is the temperature at the concrete-steel interface and  $k_s$  is the thermal conductivity of the steel beam ( $\sim 65 \text{ W m}^{-1} \text{ K}^{-1}$ ). This localised heat transfer can be up to  $150 \text{ W m}^{-2}$  during the active stage of the hydration reactions, or  $\sim 50\%$  of that at the top surface during this time (Wojcik & Fitzjarrald 2001), resulting in horizontal temperature gradients near the bottom of the deck as large as the vertical gradients at the top surface (see section 3.6).

## 2.2. Boundary condition sensitivity simulations

We examined the model's temperature, moisture, binder and heat predictions for two different categories of atmospheric boundary conditions: (i) diurnal boundary conditions (DBC) and (ii) seasonal/climate boundary conditions (SBC). The variables considered were air temperature and humidity ( $T_a$  and  $RH$ ), wind speed ( $U$ ) and cloud cover fraction ( $clf$ ). The range of values chosen represents typical conditions observed in the atmosphere (Table 2). In preliminary simulations with variations of one variable at a time, the concrete temperatures were most sensitive to  $T_a$ ,  $RH$ , and  $U$ ,

Table 2. Results of the diurnal boundary condition (DBC) model simulations for atmospheric variables when just one variable was varied at a time. The "Baseline" row gives the baseline value for each variable. The "Baseline Range" row shows the range used for each boundary value. The ranges given in the "Baseline Range" row are afternoon values except for  $clf$ . In the "Peak", "Stage III", and "Stage IV" rows are given the equations which predict these temperatures as a function of the boundary variable. The  $R^2$  value is given in parentheses underneath each equation except for  $U$  which displays the residual standard error of a polynomial fit. The temperatures in parentheses beside the titles "Peak", "Stage III", and "Stage IV" are the values for the Baseline simulation. Note that the Stage III and Stage IV temperatures are averages over the first 24 h of each stage. The "Range" rows indicate the range of predicted temperatures over the range of the given boundary variable for the temperature category given in the row above each.

	$T_a$ ( $^{\circ}\text{C}$ )	$RH$ (%)	$U$ ( $\text{m s}^{-1}$ )	$clf$
Baseline	25	70	3	0
Baseline Range	0-45 <sup>a</sup>	0-100 <sup>b</sup>	0.5-10 <sup>c</sup>	0-1
Peak (43.7 $^{\circ}\text{C}$ )	$33.5+0.48^*T_a$ (0.99)	$36.9+0.09^*RH$ (0.95)	$51.5-5.7^*U +0.57^*U^2$ (0.43)	$42.8-4.77^*clf$ (0.99)
Range	35.9-52.7	36.9-45.9	50.5-38	42.8-38.0
Stage III (30.6 $^{\circ}\text{C}$ )	$21.20+0.47^*T_a$ (0.99)	$25.0+0.08^*RH$ (0.99)	$36.0-3.2^*U +0.37^*U^2$ (0.25)	$30.2-2.5^*clf$ (0.99)
Range	23.5-40.0	25.0-33.0	35.5-27.5	30.2-27.7
Stage IV (22.6 $^{\circ}\text{C}$ )	$10.9+0.62^*T_a$ (0.99)	$16.1+0.10^*RH$ (0.99)	$28.3-3.7^*U +0.39^*U^2$ (0.39)	$22.7-2.6^*clf$ (0.99)
Range	14.0-35.7	16.1-26.1	27.9-20.3	22.7-20.1

<sup>a</sup> Afternoon-morning temperature pairs ( $^{\circ}\text{C}$ ): 45-35, 40-30, 35-25, 30-20, 25-15, 20-10, 15-5, 10-0.

<sup>b</sup> Afternoon-morning relative humidity pairs (%): 0-0, 0-60, 10-70, 20-80, 30-90, 40-100, 100-100.

<sup>c</sup> Afternoon-morning wind speed pairs ( $\text{m s}^{-1}$ ): 10-0.5, 8-0.5, 6-0.5, 4-0.5, 2-0.5, 0.5-0.5.

with peak temperatures changing by 9 °C or more over the ranges tested. Note that temperatures were nonlinearly related only to  $U$  and most sensitive to  $U$  when  $U < 2 \text{ m s}^{-1}$  (Table 2).

For the DBC simulations, typical diurnal variations of  $T_a$ ,  $RH$  and  $U$  are emulated with the following equations:

$$S_t = \bar{S} + N_S \cdot \cos\left(t \cdot \frac{2\pi}{24}\right) \quad (12)$$

where  $\bar{S}_t$  is the value of either  $T_a$ ,  $RH$  or  $U$  at time  $t$  (h);  $S$  is the daily average value of variable  $S$ ;  $N_S$  is the amplitude of the diurnal wave of the given variable:

$$N_S = \frac{S_{PM} - S_{AM}}{2} \quad (13)$$

where the subscripts PM and AM indicate the extreme values of  $S$  at 1600 and 0400 local time (LT), respectively (Figure 2). While producing smoother temporal variations of these variables than are actually encountered in the atmosphere, this formulation captures the main features of typical diurnal variations.  $T_a$  and  $U$  generally peak during the late afternoon while  $RH$  reaches a minimum during this time. Note that with this formulation,  $q_a$  in Eq. (6), is determined both as a function of  $RH$  and  $T_a$ . The DBC simulations were run for Albany, New York in early June with the concrete being placed at 0700 local time. The length of Stage II was set at eight hours. The variations of incoming solar radiation with time of day and time of year were computed with schemes discussed in section 2.1.

With the DBC, we also studied how construction practices might influence the concrete heat generation and temperatures. For these cases, we varied the volume of water sprayed onto the deck ( $W$ ), the initial tempera-

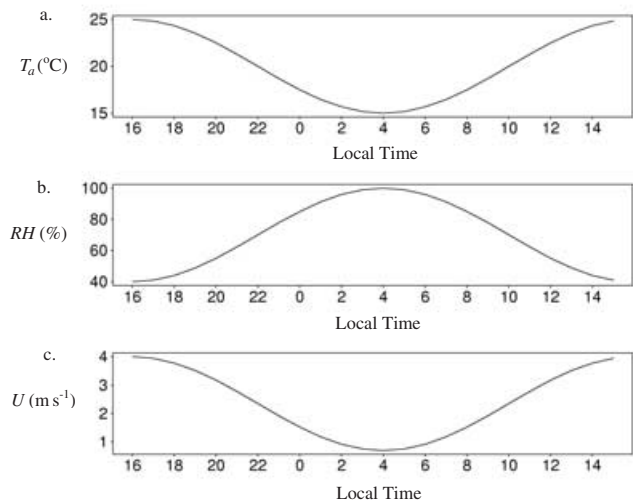


**Figure 2.** (a) Example of diurnal air temperature variations used for the diurnal boundary condition (DBC) simulations. (b) as in (a), but for relative humidity. (c) as in (a), but for wind speed.

ture of that water as it left the hoses ( $T_{d0}$ ), the concrete temperature at the time of placement ( $T_{c0}$ ) (Table 3), and the time of placement. These factors potentially can be controlled at the discretion of construction personnel or the field engineer. For the bridges we studied in the field,  $W$  ranged from 2.4 mm hr<sup>-1</sup> to 15 mm hr<sup>-1</sup>.  $T_{c0}$  for the bridges ranged from 23 °C to 29 °C and  $T_{d0}$  from 15 °C to 29 °C (initial spray water temperature data are available only for the 1998 and 1999 bridges). We expanded the ranges of these variables for the construction practice simulations to broaden the scope of our investigation. In preliminary simulations with variations of one construction variable at a time, the concrete temperatures were most sensitive to  $T_{c0}$  with peak temperatures increasing by more than 15 °C over the range tested (Table 3).

**Table 3.** Results of the diurnal boundary condition (DBC) model simulations for construction practice variables. The “Baseline” row gives the baseline value for each variable. The “Baseline Range” row shows the range used for each boundary value. In the “Peak”, “Stage III”, and “Stage IV” rows are given the equations which predict these temperatures as a function of the boundary variable, with the  $R^2$  value in parentheses underneath each equation. The temperatures in parentheses beside the titles, “Peak”, “Stage III”, and “Stage IV” are the values for the Baseline simulation. Note that the Stage III and Stage IV temperatures are averages over the first 24 h of each stage. The “Range” rows indicate the range of predicted temperatures over the range of the given boundary variable for the temperature category given in the row above each.

	$W$ (mm h <sup>-1</sup> )	$T_{c0}$ (°C)	$T_{d0}$ (°C)
Baseline	14	25	25
Baseline Range	0–52	5–40	5–40
Peak (43.7 °C)	43.7–0.062* $W$ (0.98)	32.7+0.45* $T_{c0}$ (0.99)	40.2+0.1* $T_{d0}$ (0.99)
Range	43.7–40.5	35.0–50.7	40.7–44.2
Stage III (30.6 °C)	31.2–0.054* $W$ (0.97)	25.4+0.21* $T_{c0}$ (0.99)	27.1+0.12* $T_{d0}$ (0.99)
Range	31.2–28.4	26.5–33.8	27.7–31.9
Stage IV (22.6 °C)	22.8–0.011* $W$ (0.97)	22.7–0.001* $T_{c0}$ (0.86)	18.7+0.16* $T_{d0}$ (0.99)
Range	22.8–22.2	22.7	19.5–25.1

To examine how the predicted concrete heat generation and temperatures would vary depending on the season and geographical location (SBC simulations), we used average climate data from the Northeast Regional Climate Center at Cornell University, Ithaca, NY, for Albany, New York (temperate climate), Tampa Bay, Florida (tropical), Phoenix, Arizona (desert), and Fairbanks, Alaska (cold) for the atmospheric boundary conditions. These data consist of the daily average maximum and minimum temperatures and relative humidities, and daily average wind speeds for January, April, July and October (Table 4). The time of placement was 0700 local time and the length of Stage II was set to 8 h.

For all simulations, we compared the mean concrete temperatures over the first 24 h of Stage III and Stage IV and the peak Stage III concrete temperature. In addition, we compared the peak temperature gradients in Stages III and IV and the 24 h and 72 h cumulative heat generation and hydration fractions.

### 3. Results

#### 3.1. Validation of SLABS model boundary conditions

To validate the model boundary conditions, we determined the predicted concrete temperature *RMSE* with predicted temperatures and those measured by NYS-DOT for all grids when the concrete was no longer

generating significant heat (after about 40 h after the pour) and local fluxes of heat and moisture determined the concrete's thermal structure (Stage IV). We performed simulations with the observed 1998 and 1999 conditions which, respectively, featured cloudy, cool, moist atmospheric conditions and sunny, warm, dry atmospheric conditions. We compared model predictions of the surface fluxes to the energy balance estimates for these bridges from the field work. Because up to 85% of the heat transfer above the form occurred through the top surface (Wojcik & Fitzjarrald 2001), we focused mainly on the top surface fluxes. We also evaluated the predicted heat transfer through the steel support beams where heat transfer of up to  $150 \text{ W m}^{-2}$  was observed.

For simulations of concrete temperatures over the form, the model produced *RMSE* of  $\sim 1^\circ\text{C}$  during the day and night for both bridges. Figure 3 shows predicted and observed concrete temperatures for the 1999 bridge. During the daytime,  $Q_{GA}$  was underpredicted by about 10–30%, and during the night  $Q_{GA}$  was overpredicted by  $< 30\%$ . The underprediction during the daytime was the result of overpredictions of  $-Q_{A}^*$  ( $\sim 15\%$  at peak) that enhanced  $Q_{EA}$ ,  $Q_{HA}$  and  $Q_{RA}$ .

During Stage IV above the beams, the predicted *RMSE* was about  $1.7^\circ\text{C}$  for both bridges (e.g. Figure 3). Note that the predicted temperatures over the beam during Stage III were up to  $5^\circ\text{C}$  lower than those over the form, as seen in the observations. For the 1999

Table 4. Climate information for the four cities used in the SBC model simulations. The data were obtained from the Northeast Regional Climate Center at Cornell University in Ithaca, NY USA. Temperature data are for years 1961–1990 and humidity and wind data are for at least 45 years up to 1998.

	Phoenix, AZ	Tampa, FL	Albany, NY	Fairbanks, AK
<b>July</b>				
<i>RH</i> Afternoon (%)	20	63	55	50
<i>RH</i> Morning (%)	43	87	81	69
$T_a$ Afternoon ( $^\circ\text{C}$ )	41	32	29	22
$T_a$ Morning ( $^\circ\text{C}$ )	27	23.6	15	11.4
<i>U</i> Mean Daily ( $\text{m s}^{-1}$ )	3.2	3.2	3.4	2.9
<b>October</b>				
<i>RH</i> Afternoon (%)	22	58	58	67
<i>RH</i> Morning (%)	49	89	86	79
$T_a$ Afternoon ( $^\circ\text{C}$ )	31	29	16.6	0
$T_a$ Morning ( $^\circ\text{C}$ )	16	18.4	4.6	-6.9
<i>U</i> Mean Daily ( $\text{m s}^{-1}$ )	2.6	3.8	3.6	2.4
<b>January</b>				
<i>RH</i> Afternoon (%)	32	60	63	70
<i>RH</i> Morning (%)	65	87	78	69
$T_a$ Afternoon ( $^\circ\text{C}$ )	18.8	21	-1	-18.7
$T_a$ Morning ( $^\circ\text{C}$ )	5	10	-11.7	-28
<i>U</i> Mean Daily ( $\text{m s}^{-1}$ )	2.4	3.2	4.4	1.3
<b>April</b>				
<i>RH</i> Afternoon (%)	16	52	49	45
<i>RH</i> Morning (%)	42	87	72	60
$T_a$ Afternoon ( $^\circ\text{C}$ )	29.2	27.6	14.2	5
$T_a$ Morning ( $^\circ\text{C}$ )	12.9	16	1.7	-6.4
<i>U</i> Mean Daily ( $\text{m s}^{-1}$ )	3.1	4.1	4.7	2.9

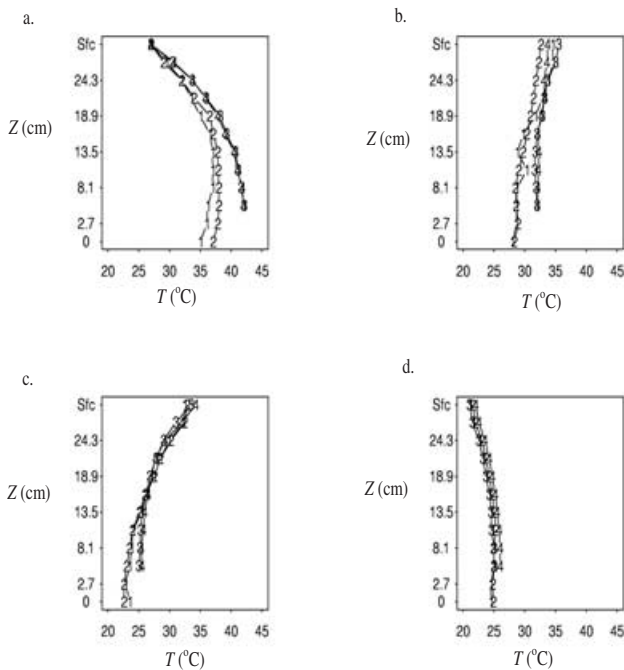


**Figure 3.** Observed and predicted vertical profiles of concrete temperatures above the beam, ‘1’ and ‘2’, respectively, and observed and predicted vertical profiles of concrete temperatures above the form, ‘3’ and ‘4’, respectively. Distances,  $Z$ , are distances above the top of the beams. ‘Sfc’ indicates the top surface. (a) At 2300 LT on 10 June 1999, the approximate time of peak concrete temperatures (Stage III); (b) as in (a), but for 1300 LT on 11 June (Stage III); (c) as in (a), but for 1300 LT on 13 June (Stage IV); (d) as in (a), but for 0200 LT on 14 June (Stage IV).

bridge, predicted heat transfer through the beams was  $25 \text{ W m}^{-2}$  during the daytime and  $-100 \text{ W m}^{-2}$  during the night, while the values estimated from the field measurements were about  $20 \text{ W m}^{-2}$  during the daytime and  $-80 \text{ W m}^{-2}$  during the night.

Because the model top surface and beam fluxes were within 30% of those determined from the field observations during most times for both bridges, and because the predicted temperatures were within  $2^\circ\text{C}$  of the observed values during the day and night, we feel our boundary condition parameterizations (in conjunction with the values for  $\rho_c$ ,  $c_{pc}$ , and  $k_c$ ; see section 3.2) are reasonable.

### 3.2. Sensitivity of predicted temperatures to model parameters

SLABS uses a set of parameters whose values are uncertain to varying degrees. The uncertainties for  $k_c$ ,  $\rho_c$  and  $c_{pc}$  are, respectively,  $\pm 30\%$ ,  $\pm 1\%$  and  $\pm 10\%$  (Wojcik & Fitzjarrald 2001) and for  $-\Delta H$  is  $\pm 15\%$  (Wojcik et al. 2001). We tested the model sensitivity to these parameters and  $K_R$  by comparing the  $RMSE$  from a simulation with a baseline set of parameter values given in section 2.1 with the  $RMSE$  from simulations with perturbation parameter values determined from the uncertainty estimates. We focused only on Stage IV

temperatures for this analysis, as we did with the boundary condition validation. For these comparisons,  $Ea=35000 \text{ J mol}^{-1}$ ,  $A=0.0039$  and  $\eta=8.3$  (see section 3.3). By varying  $k_c$  from 2 to  $4 \text{ W m}^{-1} \text{ K}^{-1}$ , the largest change in  $RMSE$  from the baseline value was  $0.8^\circ\text{C}$ . Variations of  $K_R$  from  $10^{-8}$  to  $10^{-12} \text{ m}^2 \text{ s}^{-1}$ ,  $\rho_c$  from 2100 to  $2400 \text{ kg m}^{-3}$ , and  $c_{pc}$  from 1300 to  $1460 \text{ J kg}^{-1} \text{ K}^{-1}$  changed the  $RMSE$  by at most  $0.3^\circ\text{C}$ . The largest change in  $RMSE$  from the baseline value when  $-\Delta H$  was varied from 360 to  $540 \text{ kJ kg}^{-1}$  was  $1.8^\circ\text{C}$ .

### 3.3. Determining and validating $\eta$ and $A$

To determine  $A$  and  $\eta$ , we optimised the model’s  $RMSE$  over the first 36 h of Stage III for the 1999 bridge by varying  $A$  and  $\eta$ , respectively, over the ranges of  $0.002 < A < 0.005$  and  $6.5 < \eta < 10.5$ . The optimal  $\eta$  was 8.3 and the optimal  $A$  was 0.0039, giving an  $RMSE$  of  $1^\circ\text{C}$  (Table 5). These optimal values are consistent with the work of Papadakis et al. (1992) ( $\eta=7.6$ ) when considering all binder components and the hydration products. We selected the optimal values  $\eta=8.3$  and  $A=0.0039$  for the 1999 bridge.

We tested the utility of the optimal values of  $A$  and  $\eta$  obtained for the 1999 bridge by using them for simulations of the other bridges. With no adjustments for retarder effects, the model simulations with the 1999 values resulted in  $RMSE$ s from  $1.8^\circ\text{C}$  to  $3.1^\circ\text{C}$  for the other bridges (Table 5). Given the fact that different cements, flyash, microsilica, and retarders were used at each of these bridges, these model predictions are very reasonable. When we lowered the hydration rates due to the retarder as suggested by Wojcik et al. (2001) for the 1996 bridge (which had the greatest retarder dosage), the  $RMSE$  decreased from  $3.1^\circ\text{C}$  to  $1.2^\circ\text{C}$  (Table 5). This adjustment for retarders lowered the Stage III hydration rates by 10–30%.

With  $A=0.0039$  and  $\eta=8.3$ , predicted binder hydration fractions,  $\alpha$ , were about 0.5 at 24 h and 0.52 at 72 h (Table 5). We do not have any measured estimates of  $\alpha$  with which to compare our model predictions. However, the predicted values are within the range of 0.5 to 0.75 by 72 h given by Verbeck & Foster (1950) and Bogue (1955).

By 24 h, the model predicted that 234, 193, 193 and  $220 \text{ kJ kg}^{-1}$  were liberated for the 1995, 1996, 1998 and 1999 bridges, respectively. These values are within 15% of those determined from calorimetry experiments and from energy balance estimates with field measurements (Wojcik et al. 2001; Wojcik & Fitzjarrald 2001). With the close agreement between predicted and expected hydration fractions, predicted and observed  $-\Delta H$ , and with the low  $RMSE$ , we conclude that our choices of  $A$  and  $\eta$  are reasonable.

Table 5. Information about the concrete mixes used for each bridge and the model RMSE of Stage III predicted concrete temperatures using the optimal values of  $\Lambda$  and  $\eta$  determined for the 1999 bridge. For the 1996 and 1998 bridges, the “Predicted Peak Temperatures”, “ $\alpha$  (24 h)”, and “ $\alpha$  (72 h)” were obtained with the simulations that included a retarder adjustment.

	1995	1996	1998	1999
Concrete Type	Class H	Class HP	Class HP	Class HP
$-\Delta H$ (kJ kg <sup>-1</sup> )	460	395	395	430
Initial Concrete Temperature (°C)	29	25	23	23
Retarder (oz. (100 lb cementitious solids) <sup>-1</sup> )	4	5.8	5	4
RMSE no retarder (°C)	2.4	3.1	1.8	1.0
RMSE with retarder (°C)	—	1.2	1.7	—
Predicted Peak Temperature (°C)	54	33	36	42
Observed Peak Temperature (°C)	55	32	37	43
$\alpha$ (24 h)	0.51	0.49	0.49	0.51
$\alpha$ (72 h)	0.52	0.52	0.51	0.53

### 3.4. Concrete temperatures with diurnal boundary conditions (DBC)

Note that for the DBC results, unless otherwise stated,  $T_a$ ,  $RH$  and  $U$  are given as the afternoon values (see Table 2), i.e.  $T_a$  and  $U$  are daily maxima and  $RH$  is the daily minimum. The highest concrete temperatures occurred at higher  $T_a$  and  $RH$  and at lower  $clf$  and  $U$  (Figures 4–6). While we recognise that  $RH$  is a function of  $T_a$ , we plotted  $RH$  instead of  $q_a$  because  $RH$  is a more familiar variable to construction personnel and engineers who may be interested in the work we are

presenting here. The peak and mean Stage III and IV concrete temperatures can vary by up to 35 °C depending on ambient conditions. These temperature predictions show that atmospheric conditions strongly influence curing concrete temperatures both in the active and passive states and therefore, will influence the long-term durability of the concrete. The extent of this influence is currently a topic of research at the Building and Fire Research Laboratory at the National Institute of Standards and Technology in Gaithersburg, Maryland, USA.

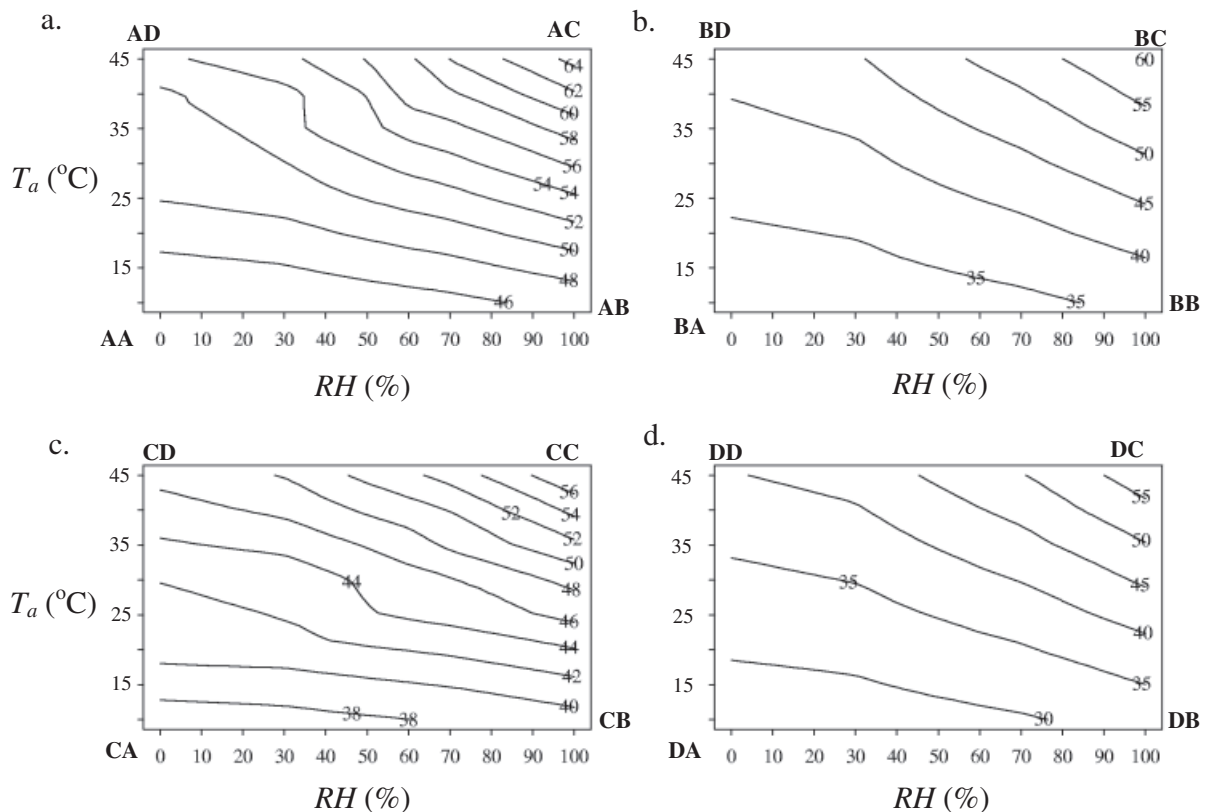


Figure 4. (a) Predicted peak concrete temperatures in Stage III from the diurnal boundary condition (DBC) simulations as a function of afternoon  $RH$  and  $T_a$ , with  $U = 0.5 \text{ m s}^{-1}$  and  $clf = 0$ . All other variables are set to baseline values as shown in Tables 2 and 3. (b) as in (a), but with  $U = 5 \text{ m s}^{-1}$ ; (c) as in (a), but with  $clf = 1$ ; (d) as in (a), but with  $U = 5 \text{ m s}^{-1}$  and  $clf = 1$ .

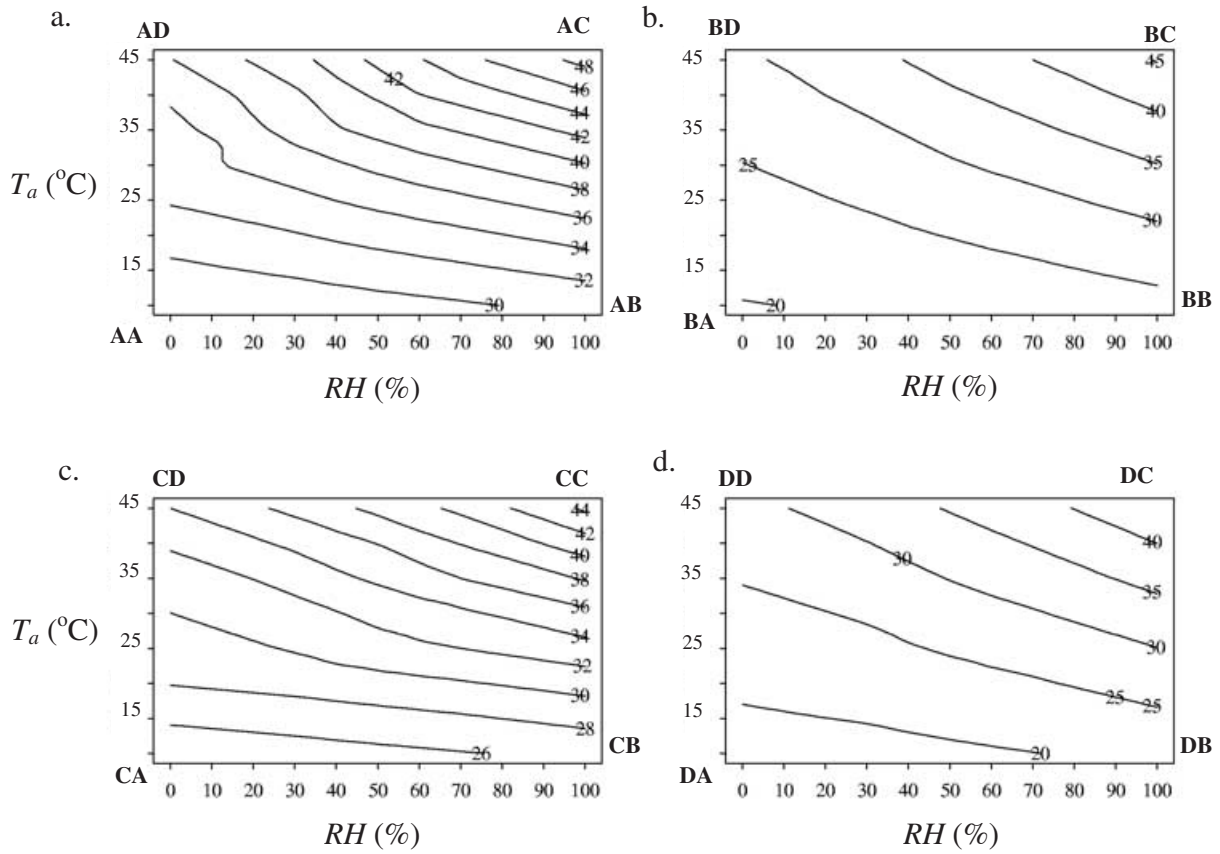


Figure 5. As Figure 4, but for mean Stage III temperatures.

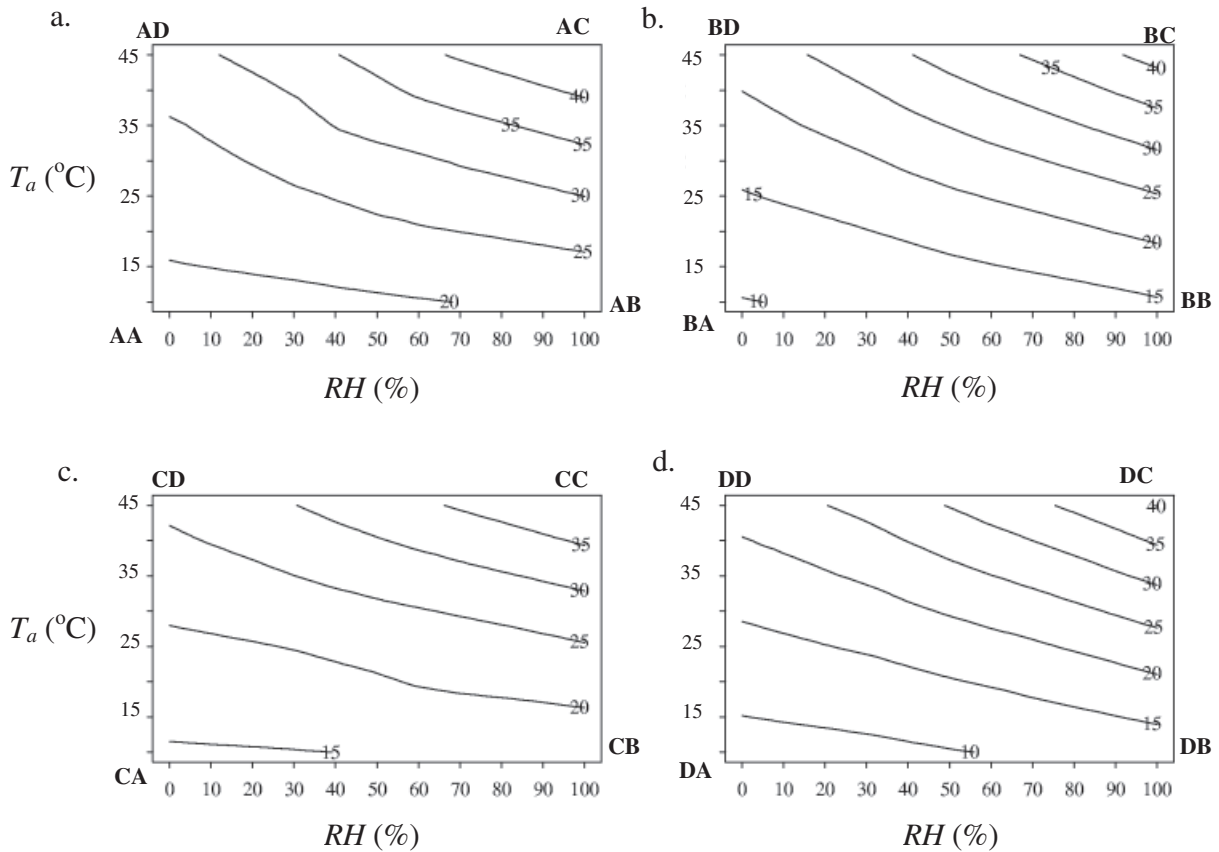


Figure 6. As Figure 4, but for mean Stage IV temperatures.

The highest peak temperature (64°C) under the atmospheric conditions considered occurred at  $T_a=45^\circ\text{C}$ ,  $RH=100\%$ ,  $U=0.5\text{ m s}^{-1}$  and  $clf=0$ . Under these same conditions, the mean Stage III and IV temperatures were 49°C and 45°C, respectively. With the same  $T_a$  and  $RH$  but at  $clf=1$  and  $U=5\text{ m s}^{-1}$ , the peak temperature decreased to 55°C as the higher  $U$  enhanced the convective fluxes and higher  $clf$  reduced incoming radiation (Table 6; see section 3.5 for a more detailed investigation of energy balances in different conditions).

Note that when  $U$  was increased, the peak concrete temperatures in the range of 58°C to 64°C decreased 4°C to 6°C while those peak concrete temperatures from 46°C to 54°C decreased 10°C or more (Figure 4). The temperature-dependent hydration reactions overwhelmed the boundary influences when the concrete temperatures were higher. At the lower concrete temperatures, the hydration reactions were slower which reduced the temperatures of the bulk concrete and allowed the boundary influences to be more prominent. Therefore, the boundary conditions play a stronger role in determining concrete temperatures at lower concrete temperatures. Similar results were found for the average Stage III temperatures (Figure 5).

Concrete temperatures also are influenced strongly by construction practices as peak and mean Stage III temperatures can vary by 20°C or more (Figures 7 and 8). This finding suggests that the effects of adverse atmospheric conditions on curing concrete potentially can be mitigated by altering construction practices.

The highest concrete temperatures for the construction conditions occurred when  $T_{co}=40^\circ\text{C}$  and  $W=0\text{ mm h}^{-1}$

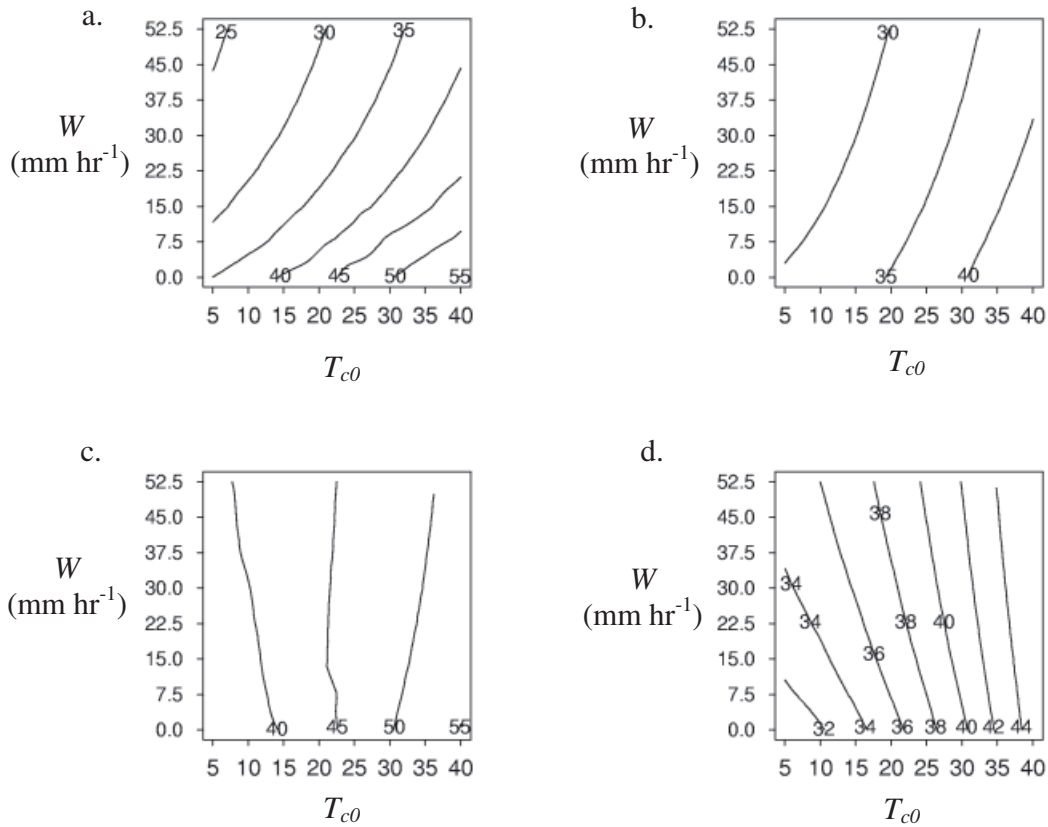
(Figures 7 and 8). With higher  $T_{co}$  and with no spray water ( $Q_{RA}=0$ ), concrete temperatures were higher and the hydration reactions were faster. Note that when  $W\neq 0$ ,  $T_{do}$  is an important influence on the concrete temperatures. At  $T_{co}=40^\circ\text{C}$ ,  $W=52.5\text{ mm h}^{-1}$  and  $U=0.5\text{ m s}^{-1}$ , when  $T_{do}$  was increased from 5°C to 40°C, the peak concrete temperatures increased from 38°C to 53°C as  $Q_{RA}$  was reduced. With a minimal heat source, the mean Stage IV concrete temperatures are not influenced by  $T_{co}$ .

When both construction and atmospheric conditions were selected to give the maximum concrete temperatures, the peak temperature and the Stage III and IV mean temperatures were, respectively, 73°C, 55°C and 49°C.

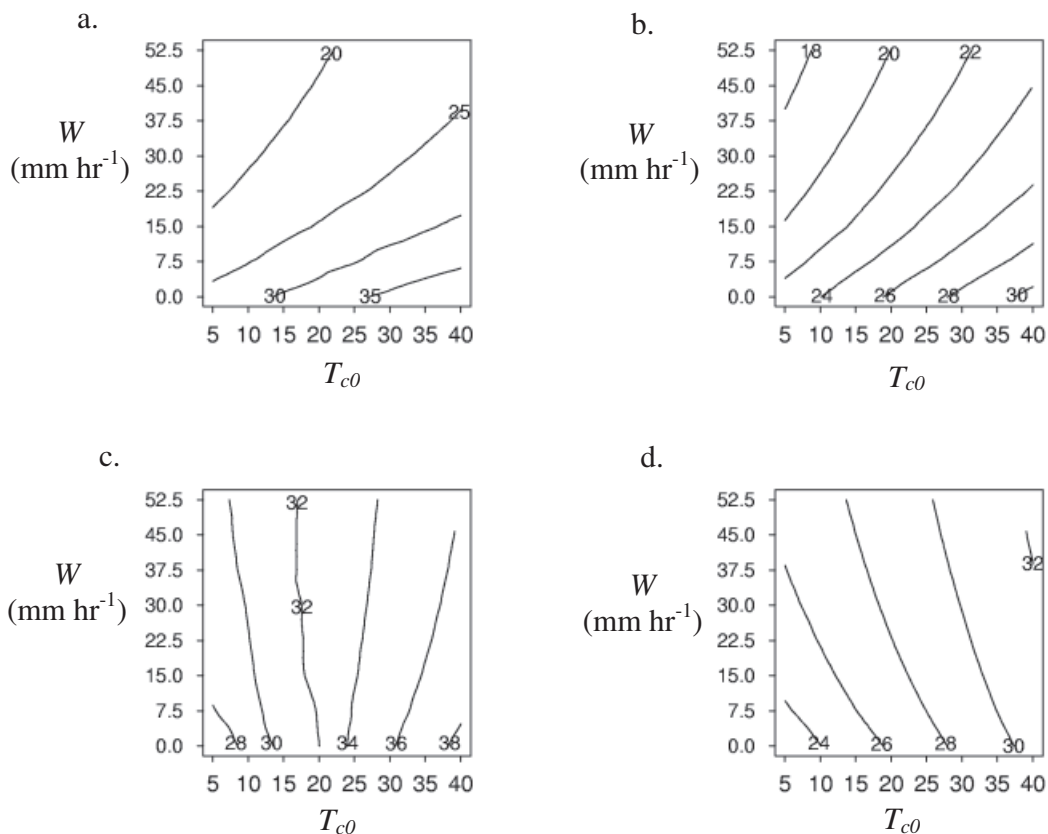
The vertical profile of the hydration fraction,  $\alpha$ , at 72 h generally had values up to 0.7 near the top surface and 0.45 near the bottom of the deck, consistent with the vertical profile of  $R$  which peaks at the top surface (where the spray water was a source) and was a minimum near the bottom of the bridge deck. The small  $R$  away from the top two grids occurred because the initial  $R$  in the concrete mix was used in the hydration process and very little was replenished from above due to the relatively slow diffusion of water. Without efficient penetration of water below the top 5 cm (top two grids), as supported by Bentz (2002), there may be a wide range of  $\alpha$  vertically within the deck which suggests variations in strength and durability depending on location. We do not have any direct measurements of  $\alpha$  from any of the bridges to confirm our model results.

Table 6. Average top surface energy balance terms ( $\text{W m}^{-2}$ ) over the first 24 h of Stage III for the diurnal boundary condition (DBC) simulations for points indicated on Figure 4. For example, on Figure 4a, AA is at  $T_a=10^\circ\text{C}$  and  $RH=0\%$ ; AB is at  $T_a=10^\circ\text{C}$  and  $RH=100\%$ ; AC is at  $T_a=45^\circ\text{C}$  and  $RH=100\%$ ; and AD is at  $T_a=45^\circ\text{C}$  and  $RH=0\%$ .

	$-Q_{GA}$	$Q_{RA}$	$Q_{EA}$	$Q_{HA}$	$-Q_A^*$
AA	238	98	162	65	87
AB	223	107	145	78	107
AC	161	190	176	23	228
AD	210	186	210	-22	169
BA	267	-40	350	97	139
BB	251	-7	246	164	153
BC	193	126	284	41	259
BD	314	72	705	-246	216
CA	236	55	122	52	-6
CB	228	55	95	60	-17
CC	147	132	57	9	51
CD	197	172	181	-23	133
DA	251	-60	291	57	36
DB	240	-31	165	122	15
DC	156	109	94	14	62
DD	313	77	668	-259	172



**Figure 7.** (a) Peak concrete temperatures from the diurnal boundary conditions (DBC) simulations when  $W$  and  $T_{c0}$  were varied.  $T_{d0} = 5^\circ\text{C}$  and mean daily  $U = 0.5 \text{ m s}^{-1}$ . All other variables were kept at the Baseline values as given in Tables 2 and 3. (b) as in (a), but for mean daily  $U = 5 \text{ m s}^{-1}$ ; (c) as in (a), but with  $T_{d0} = 40^\circ\text{C}$ ; (d) as in (a), but with mean daily  $U = 5 \text{ m s}^{-1}$  and  $T_{d0} = 40^\circ\text{C}$ .



**Figure 8.** As Figure 7, but for mean Stage III temperatures.

### 3.5 Top surface energy balances for the diurnal boundary conditions

We examined the average top surface energy balance terms (Eq. 5) over the first 24 h of Stage III for DBC in Figures 4 and 5. All terms of the balance were significant and varied depending on the ambient conditions (Table 6), as was found by Wojcik & Fitzjarrald (2001) from the field work. The largest  $Q_{EA}$  occurred when  $U=5 \text{ m s}^{-1}$ ,  $T_a=45^\circ\text{C}$  and  $RH=0\%$  under clear skies (BD in Table 6 and Figure 4). In these conditions, the higher surface to air humidity difference and wind speeds produced efficient heat loss from the concrete by evaporation.

$Q_{RA}$  was maximum at  $U=0.5 \text{ m s}^{-1}$  and  $RH=100\%$  with clear skies (AC). With light winds and low surface to air humidity differences, evaporation was limited and heat was removed more efficiently by the spray water running off the bridge, as surmised by Wojcik & Fitzjarrald (2001). At  $T_a=10^\circ\text{C}$ ,  $RH=0\%$  and  $U=5 \text{ m s}^{-1}$  (BA), the spray water added heat to the concrete (negative  $Q_{RA}$ ) as the convective terms removed enough heat to decrease the surface concrete temperature below that of the spray water.

Sensible heat was also added to the concrete ( $Q_{HA}$  negative) at  $T_a=45^\circ\text{C}$ ,  $U=5 \text{ m s}^{-1}$  and  $RH=0\%$  under clear skies (BD). With low humidities and large  $-Q_{EA}^*$ , evaporation was enhanced, cooling the surface concrete temperatures to below  $45^\circ\text{C}$ . With the higher wind speeds, there was effective transfer of sensible heat to the concrete. Under the same  $T_a$  and  $U$  conditions, but with  $RH=100\%$  (BC), evaporation was less efficient and so the concrete temperatures were higher than  $40^\circ\text{C}$ . In this instance, more heat was lost through sensible heat convection and less by evaporation than at BD. In general,  $Q_{HA}$  was maximum (removed heat from the concrete) at low  $T_a$ , high  $U$  and high  $RH$  when surface to air temperature differences were largest.

As expected,  $-Q_{EA}^*$  peaked under clear skies and high  $T_a$  and  $RH$  (AC and BC). With clear skies,  $K_I$  dominated the components of  $-Q_{EA}^*$ . With  $U=0.5 \text{ m s}^{-1}$  and high  $T_a$  and  $RH$  (AC), convective heat loss was constrained and concrete temperatures were higher than when  $U=5 \text{ m s}^{-1}$ . With higher surface temperatures, more heat was lost to radiative cooling which lowered  $-Q_{EA}^*$  (AC) in comparison to that when  $U=5 \text{ m s}^{-1}$  (BC).

Under clear skies, the incoming solar radiation,  $K_I$ , added more heat to the concrete than under cloudy skies, and as a result,  $-Q_{GA}$  was generally higher than under cloudy conditions. During Stage IV, the mean daily  $-Q_{GA}$  approaches zero as would be expected for a passive surface.

Note that hydration heat generation rates during Stage III may average about  $3 \text{ J kg}^{-1} \text{ s}^{-1}$ . This rate is

equivalent to a heat flux of of  $\sim 300 \text{ W m}^{-2}$  which is comparable to  $Q_{GA}$ ,  $Q_{RA}$ ,  $Q_{EA}$  and  $Q_{EA}^*$  over Stage III as indicated in Table 6.

### 3.6 Concrete temperature gradient sensitivity

Excessive temperature gradients in concrete,  $\Delta T_c$ , can produce thermal stresses and cracking, especially during the first several days after placement. For many years, a top to bottom concrete temperature difference ( $\Delta T_{tb}$ ) of  $\geq 20^\circ\text{C}$  for slabs  $\sim 30 \text{ cm}$  thick was used as a rule of thumb for when thermal cracking may occur. Recent work has shown that rules-of-thumb relating temperature gradients to cracking potential may not be sufficiently reliable (Emborg 1990; Roelfstra et al. 1994; Mangold & Springenschmid 1994). But since temperature gradients are an important part of stress development, we examined the sensitivity of  $\Delta T_c$  and  $\Delta T_{tb}$  to atmospheric and construction conditions.

During Stage III,  $\Delta T_c$  and  $\Delta T_{tb}$  were most sensitive to  $T_{co}$  and  $T_a$ . The largest Stage III  $\Delta T_c$  magnitudes above the form occurred at the top surface, as expected since most of the heat transfer occurred here.  $\Delta T_c$  ranged from  $-2^\circ\text{C cm}^{-1}$  to  $1^\circ\text{C cm}^{-1}$  (Figure 9a), with the largest magnitudes at  $T_{co}=40^\circ\text{C}$  and  $T_a=10^\circ\text{C}$ , when high surface temperatures due to the hydration reactions and low  $T_a$  produced efficient heat loss. The largest  $\Delta T_{tb}$  ranged from  $-25^\circ\text{C}$  to  $19^\circ\text{C}$  (Figure 9b). When  $T_{co} > 20^\circ\text{C}$  and  $T_a < 35^\circ\text{C}$ ,  $|\Delta T_{tb}|$  may exceed  $20^\circ\text{C}$ , potentially inducing excessive thermal stresses.

The peak magnitudes of these gradients occurred near the time of peak concrete temperatures or about five to eight hours into Stage III. At  $T_{co} < 10^\circ\text{C}$  and  $T_a > 25^\circ\text{C}$ , the gradients switched sign as the warm atmosphere and slower hydration reactions produced warmer temperatures at the top surface than at lower concrete levels.

While the steel support beams removed considerable heat from the concrete near the bottom of the slab, the peak  $\Delta T_c$  over the beams also occurred at the top surface and were of similar magnitude and sign of those at the top surface above the form, consistent with the observed data. Preliminary work with a 2D (horizontal and vertical) curing concrete model shows that the horizontal temperature gradients caused by heat transfer through the beams are of the same magnitude as the vertical gradients discussed above (locations of maximum horizontal gradients are marked as 'X' in Figure 1a). Therefore, thermal cracking may occur not only near the top surface where the vertical gradients peak but also near the bottom of the deck due to heat transfer through the beams.

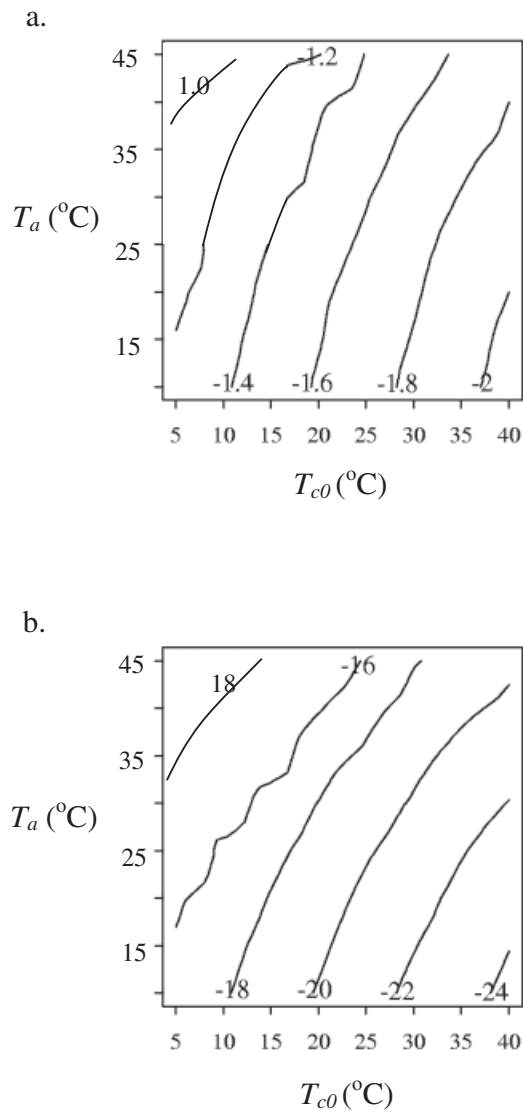


**Figure 9.** (a) Peak Stage III  $\Delta T_c$  ( $^{\circ}\text{C cm}^{-1}$ ) as a function of afternoon  $T_a$  and  $T_{c0}$ . All other variables were set to the Baseline values given in Tables 2 and 3. (b) Peak Stage III  $\Delta T_{ib}$  ( $^{\circ}\text{C}$ ) as a function of afternoon  $T_a$  and  $T_{c0}$ . All other variables were set to the Baseline values given in Tables 2 and 3.

### 3.7 Concrete temperature sensitivity to local time of pour (LTP)

Because atmospheric variables exhibit diurnal variations, there is a preferred time of day to pour concrete that will result in the lowest possible concrete temperatures and temperature gradients. The lowest concrete temperatures and temperature gradients occurred when the LTP ranged from 1300 to 2000 LT. The highest temperatures occurred for LTP between 0300 LT to 0800 LT. When  $T_a=10^{\circ}\text{C}$ , the peak concrete temperature for LTP=0700 LT was  $38^{\circ}\text{C}$  and was  $32^{\circ}\text{C}$  when LTP=1600 LT (Figure 10a). When LTP=1600 LT, the concrete temperatures at the start of Stage III were lower than that for LTP=0700 LT (Figure 10b), as local convective and runoff fluxes in the late afternoon removed more heat than was contributed from  $Q_A^*$ . Subsequent hydration reactions were slower for

LTP=1600 LT, resulting in lower Stage III concrete temperatures. Placing the concrete late in the afternoon minimised the effect of solar radiation, the dominant term in the energy balance, on the concrete's heat development. Therefore, the current NYSDOT practice of placing bridge decks early in the morning may not result in the strongest, most durable decks.

### 3.8 Concrete temperatures in different seasons and climates (SBC)

For the four cities studied, the highest peak and mean Stage III concrete temperatures occurred in July and the lowest in January, while little difference was found between April and October (Table 7). Higher air temperatures, higher atmospheric water vapour concentrations (Table 4), and larger  $K_I$  allowed the concrete to reach higher temperatures during July due to more rapid hydration in Stage III, as was seen with the DBC results.

Tampa had the highest concrete temperatures, reaching a peak of  $47^{\circ}\text{C}$  in July. Phoenix, while experiencing higher air temperatures than Tampa in July also experienced lower RH. Under these conditions,  $Q_{HA}$  at Phoenix was negative, i.e. heat was added to the concrete from the air (Table 8). With this excess heat from the air and a greater surface to air humidity difference,  $Q_{EA}$  was on average  $230 \text{ W m}^{-2}$  higher at Phoenix than at Tampa. With  $Q_{EA}$  compensating for  $Q_{HA}$  at Phoenix and the other terms in the top surface balances for these cities being approximately equal, the concrete temperatures for these two cities were approximately equal.

Concrete temperatures and  $Q_{HA}$  in January at Albany and Fairbanks were similar, despite large differences in ambient conditions (Tables 4, 7 and 8). The similarity of  $Q_{HA}$  for these cities resulted from larger surface to air temperature differences at Fairbanks than at Albany ( $-26^{\circ}\text{C}$  as against  $-10^{\circ}\text{C}$ ) that nearly compensated for the lower  $U$  at Fairbanks ( $1.3 \text{ m s}^{-1}$  compared to  $4 \text{ m s}^{-1}$ ) (Table 8). With lower  $U$ , evaporation was less efficient at Fairbanks than at Albany. So at Fairbanks, which also had less  $K_I$  than Albany ( $40 \text{ W m}^{-2}$  compared to  $140 \text{ W m}^{-2}$ ), more heat was lost at the top surface by radiative cooling, averaging  $164 \text{ W m}^{-2}$  over Stage III, than at Albany.

Because the energy balance terms vary widely depending on location, location-specific placement and curing specifications may be necessary. For example, the importance of moist curing as soon as possible after placement in warm, dry climates is underscored by the large magnitude of  $Q_{EA}$  for Phoenix in July. In locations with colder climates, such as Fairbanks, the influence of the LTP may not be important since concrete temperatures in the colder climates are considerably lower than those in the warmer climates.

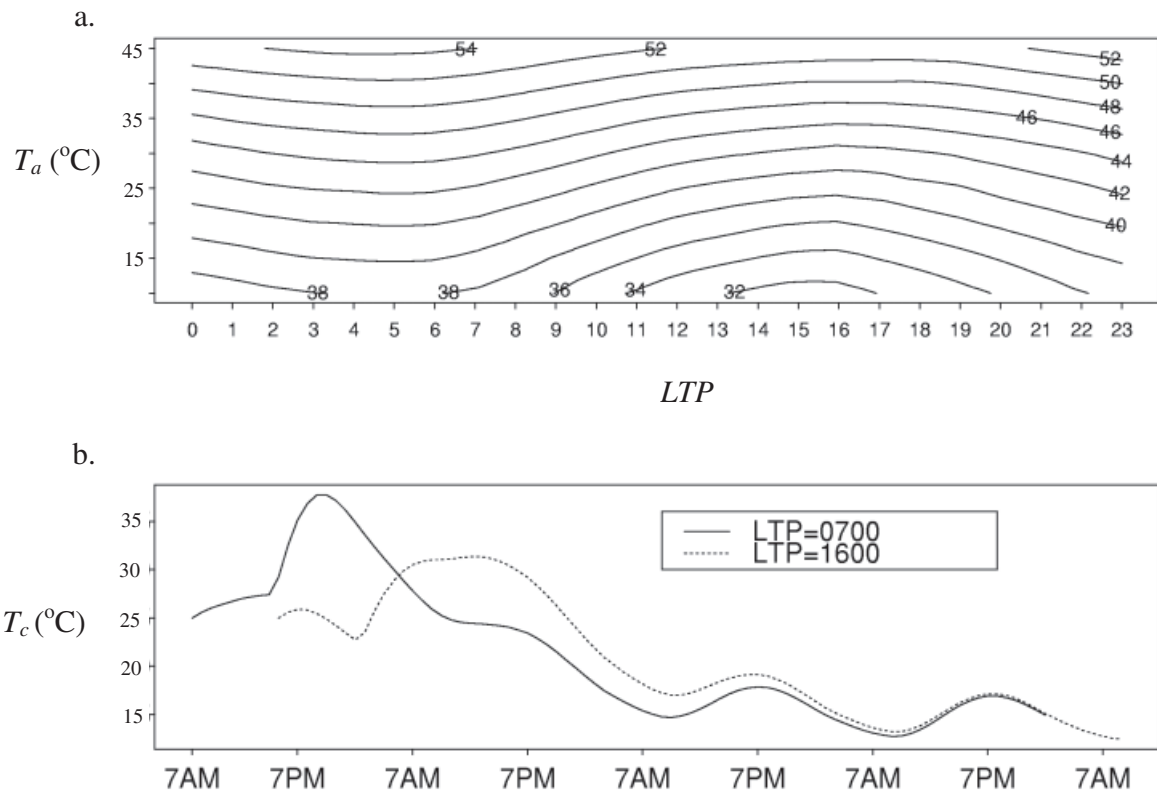


**Figure 10.** (a) Peak concrete temperatures as a function of afternoon  $T_a$  and LTP; (b) Time series of concrete temperatures ( $T_c$ ) at the bottom of the bridge deck for LTP=0700 LT and LTP=1600 LT at afternoon  $T_a=10^\circ\text{C}$ .

Table 7. Concrete temperatures ( $^\circ\text{C}$ ) predictions for the four cities examined in the seasonal and climate simulations (SBC). The “Average Stage III” temperatures were computed by averaging the concrete temperatures over all grids for the first 24 h of Stage III.

	Phoenix, AZ	Tampa, FL	Albany, NY	Fairbanks, AK
<b>July</b>				
Stage III Peak	45	47	43	39
Average Stage III	32	34	30	27
<b>October</b>				
Stage III Peak	39	42	33	25
Average Stage III	27	30	22	15
<b>January</b>				
Stage III Peak	34	36	21	21
Average Stage III	22	25	11	10
<b>April</b>				
Stage III Peak	38	41	31	28
Average Stage III	26	29	20	17

### 3.9 SLABS as an operational forecast model

As an operational forecast model, SLABS is modified to read in meteorological forecasts from the Nested Grid Model (NGM) Model Output Statistics (MOS) (Jacks et al. 1990) from the United States National Weather Service. The NGM MOS provides forecasts for every three hours up to 54 h, initialised at 0 UTC and 1200 UTC at 204 cities across the United States, including Albany, Utica and Syracuse in NY. The meteorological data that are needed are air temperature and humidity, wind speed, cloud cover and precipitation amounts. The 3 h forecasts of  $T_a$ ,  $RH$ ,  $U$  and  $clf$  are

linearly interpolated to hourly values. The hourly precipitation amounts were determined by averaging the six-hour quantitative precipitation forecast over the six-hour period. The user can specify certain conditions and parameter values such as simulations over the form or the beam, the concrete mix design (amount of binder, mix water),  $T_{c0}$ , latitude and longitude of the bridge, hydration chemistry variables, and bridge and beam dimensions.

The model executes 24 h simulations (covering hydration Stages II and III) with the LTP incremented by one hour for each simulation, starting at the first NGM

Table 8. Predicted average top surface energy balance terms ( $W m^{-2}$ ) for each city used in the season/climate simulations (SBC), averaged over the first 24 h of Stage III for July and January.

	Phoenix, AZ	Tampa, FL	Albany, NY	Fairbanks, AK
<b>July</b>				
$-Q_{GA}$	222	186	227	217
$Q_{RA}$	66	70	42	18
$Q_{EA}$	630	396	408	354
$Q_{HA}$	-196	-2	-2	33
$-Q^*_{A}$	277	256	221	189
<b>January</b>				
$-Q_{GA}$	230	223	250	234
$Q_{RA}$	-29	-18	-174	-160
$Q_{EA}$	264	291	196	69
$Q_{HA}$	13	14	185	160
$-Q^*_{A}$	19	64	-42	-164

MOS data point. With the 24 h simulations, the model performs 31 simulations (31 possible *LTP*) of the same duration given each NGM MOS forecast.

The outputs of the model are written to the screen and to a file in table form and include the *LTP*, the peak concrete temperature, peak  $\Delta T_c$ , peak  $\Delta T_{tb}$ , and  $Q_{EA}$  over the first 3 h of the pour (Figure 11). Four warning messages about potentially damaging conditions (based on NYSDOT specifications) are also output when appropriate. These are:

- when an 1 h evaporation rate during the first 3 h of the pour exceeds  $830 W m^{-2}$ ;
- when the air temperature is at or below  $7^\circ C$ ;
- when any concrete temperature falls to or below  $0^\circ C$ ; and
- when precipitation is predicted during the first 3 h of the pour.

The output messages contain the day and time of the occurrence of each of these conditions.

For the 1200 UTC NGM MOS forecast for Albany (50 km east of the 1999 bridge) from 9 June 1999 (the day before the pour of the 1999 bridge), the model predicted that the highest peak concrete temperatures,  $|\Delta T_c|$ , and  $|\Delta T_{tb}|$  would occur when *LTP* was early in the morning and the lowest when *LTP* was late afternoon or early evening (Figure 11), as was seen with the DBC results. The field engineer did have *LTP* options that could have resulted in lower concrete temperatures,  $\Delta T_c$  and  $\Delta T_{tb}$ . Note that no adverse conditions occurred in these simulations (i.e. no warning messages).

For *LTP*=1000 LT on 10 June 1999 (the time the concrete reached our sensors at the 1999 bridge), the predicted peak temperature was  $\sim 38^\circ C$ , or  $5^\circ C$  lower than observed (Table 5) and occurred two hours before the observed peak. The overall Stage II and Stage III concrete temperature *RMSE* for this *LTP* averaged

$5^\circ C$ . The primary reason for this underprediction was that the NGM MOS-predicted  $U$  was two times larger than the observed during the daytime ( $4 m s^{-1}$  compared to  $2 m s^{-1}$ ) and four times larger than the observed at night ( $2.8 m s^{-1}$  compared to  $0.7 m s^{-1}$ ).

Many large trees (up to 15 m tall) and several buildings 100 m upwind of the 1999 bridge acted as windbreaks and reduced the wind speed from the condition of no obstacles (e.g. Fujita & Wakimoto 1982; Acevedo 2001). We lowered the NGM MOS wind forecasts by a factor of 3 based on work by Acevedo (2001) accounting for the effects of windbreaks on local wind speeds by relating the obstruction angles (angle from the observation point to the top of the obstacle) to a transmission factor. With this corrected  $U$ , the overall Stage II and Stage III *RMSE* for *LTP*=1000 was reduced from  $5^\circ C$  to  $2^\circ C$  and the predicted peak temperature increased from  $38^\circ C$  to  $43^\circ C$ , identical to the observed (Table 5). Therefore, a field engineer could estimate the obstruction angle and determine a transmission factor at a given location to augment the NGM MOS forecast to provide more accurate concrete temperature forecasts.

### 3.10 Comments on current curing and placement specifications

Without more information about the interaction between concrete stress development and concrete temperatures during the first few days after placement, we cannot draw conclusions about the utility of current curing and placement specifications in ensuring high quality concrete. However, we offer some comments about these specifications and related information based on the present work.

Because the NYSDOT requires that moist curing be used on all bridge decks and that the moist curing begin within 30 minutes of placement, the evaporation specification for  $Q_{EA} < 830 W m^{-2}$  at the time of placement

```

*****
NGM MOS Forecast Beginning: 6/ 9 at Local Time: 14
*****
*****
Pour Time      Peak T      Peak TG      Peak TBD      Evap Rate
mm  dd  lt      C          C/cm         C          W/m2
*****
6   9   14      36.6       -1.16        -13.8       210.
Warning Messages: None
-----
6   9   15      35.5       -1.02        -13.5       218.
Warning Messages: None
-----
6   9   16      35.2       -1.00        -13.1       225.
Warning Messages: None
-----
6   9   17      35.0       -0.98        -12.7       234.
Warning Messages: None
-----
6   9   18      35.0       -0.94        -12.2       233.
Warning Messages: None
-----
6   9   19      35.1       -0.90        -11.5       225.
Warning Messages: None
-----
6   9   20      35.4       -0.92        -11.2       209.
Warning Messages: None
-----
6   9   21      35.9       -1.01        -12.4       198.
Warning Messages: None
-----
6   9   22      36.3       -1.06        -13.2       188.
Warning Messages: None
-----
6   9   23      36.7       -1.11        -13.8       185.
Warning Messages: None
-----
6  10   0      37.1       -1.16        -14.5       175.
Warning Messages: None
-----
6  10   1      37.6       -1.21        -15.3       168.
Warning Messages: None
-----
6  10   2      38.0       -1.27        -16.0       149.
Warning Messages: None
-----
6  10   3      38.4       -1.32        -16.7       140.
Warning Messages: None
-----
6  10   4      38.7       -1.38        -17.4       134.
Warning Messages: None
-----
6  10   5      38.9       -1.42        -18.0       150.
Warning Messages: None
-----
6  10   6      38.9       -1.46        -18.5       172.
Warning Messages: None
-----
6  10   7      38.8       -1.48        -19.0       204.
Warning Messages: None
-----
6  10   8      38.7       -1.49        -19.1       260.
Warning Messages: None
-----
6  10   9      38.3       -1.49        -18.9       332.
Warning Messages: None
-----
6  10  10      37.7       -1.47        -18.6       407.
Warning Messages: None
-----
6  10  11      37.0       -1.39        -17.6       462.
Warning Messages: None
-----
6  10  12      36.2       -1.29        -16.6       487.
Warning Messages: None
-----
6  10  13      35.4       -1.20        -15.9       477.
Warning Messages: None
-----
6  10  14      34.8       -1.19        -15.6       449.
Warning Messages: None
-----
6  10  15      34.2       -1.17        -15.1       415.
Warning Messages: None
-----
6  10  16      33.7       -1.11        -14.2       376.
Warning Messages: None
-----
6  10  17      33.5       -1.04        -13.2       333.
Warning Messages: None
-----
6  10  18      34.3       -0.91        -11.9       303.
Warning Messages: None
-----
6  10  19      35.0       -0.79        -10.3       291.
Warning Messages: None
-----
6  10  20      35.8       -0.83         -9.9       303.
Warning Messages: None
-----

```

Figure 11. (Left) Output file generated by the SLABS operational forecast model.

(Table 1) may not be necessary. The NYSDOT mandates the use of a nomogram to determine the evaporation rate based on  $T_a$ ,  $RH$ ,  $U$ , and  $T_{co}$ . Our evaporation parameterisation predicts values 15–35% higher than those given in the nomogram.

Generally,  $Q_{EA}$  increases for decreasing  $T_a$  and  $RH$  and increasing  $U$  and  $T_{co}$  (Figure 12). When  $Q_{EA} > 0$ , a 10°C increase in  $T_{co}$  increased  $Q_{EA}$  by a factor of 2–2.5. Evaporation rates can often exceed 680 W m<sup>-2</sup> (the ACI critical rate) which emphasises the need for moist curing and the need for considering atmospheric and construction conditions when deciding the best time to pour. In addition, restricting the pour to early morning to limit evaporation may not be necessary since  $Q_{EA} < 680$  W m<sup>-2</sup> for many typical afternoon conditions.

To keep concrete temperatures and temperature gradients in Stage III as low as possible, the concrete should be moist-cured (already required for NYSDOT bridge decks),  $T_{co}$  should be kept as low as possible (< 25°C), and the concrete should be poured in the late afternoon under typical conditions. In general, NYSDOT should consider specifications for  $T_{co}$ ,  $LTP$ ,  $T_a$ ,  $RH$  and  $U$  and should remove that for  $Q_{EA}$  since they require moist curing within 30 minutes of placement. Because of the complexity of the interactions among all the atmospheric and construction variables and the concrete, NYSDOT also should require the use of the SLABS forecast model to provide the engineer with specific information about the conditions that may be experienced on site.

## 4. Conclusions and discussion

### 4.1. Conclusions

In this paper, we described and applied a 1D model, SLABS, to predict the temperatures and water and binder concentrations of freshly-placed, hydrating Class HP concrete. We have investigated the effects of atmospheric conditions and construction practices on these concrete states, with the following important results:

1. During Stage IV of the hydration process when the concrete is generating little heat, the model predictions of concrete temperatures were within 2°C of the observed temperatures above both the form and the beams. Predicted energy balances at the top surface were within 30% of those determined from field observations. These findings validate the boundary condition parameterisations and the model’s physical parameters.
2. The highest concrete temperatures occurred at high air temperatures and humidities and initial

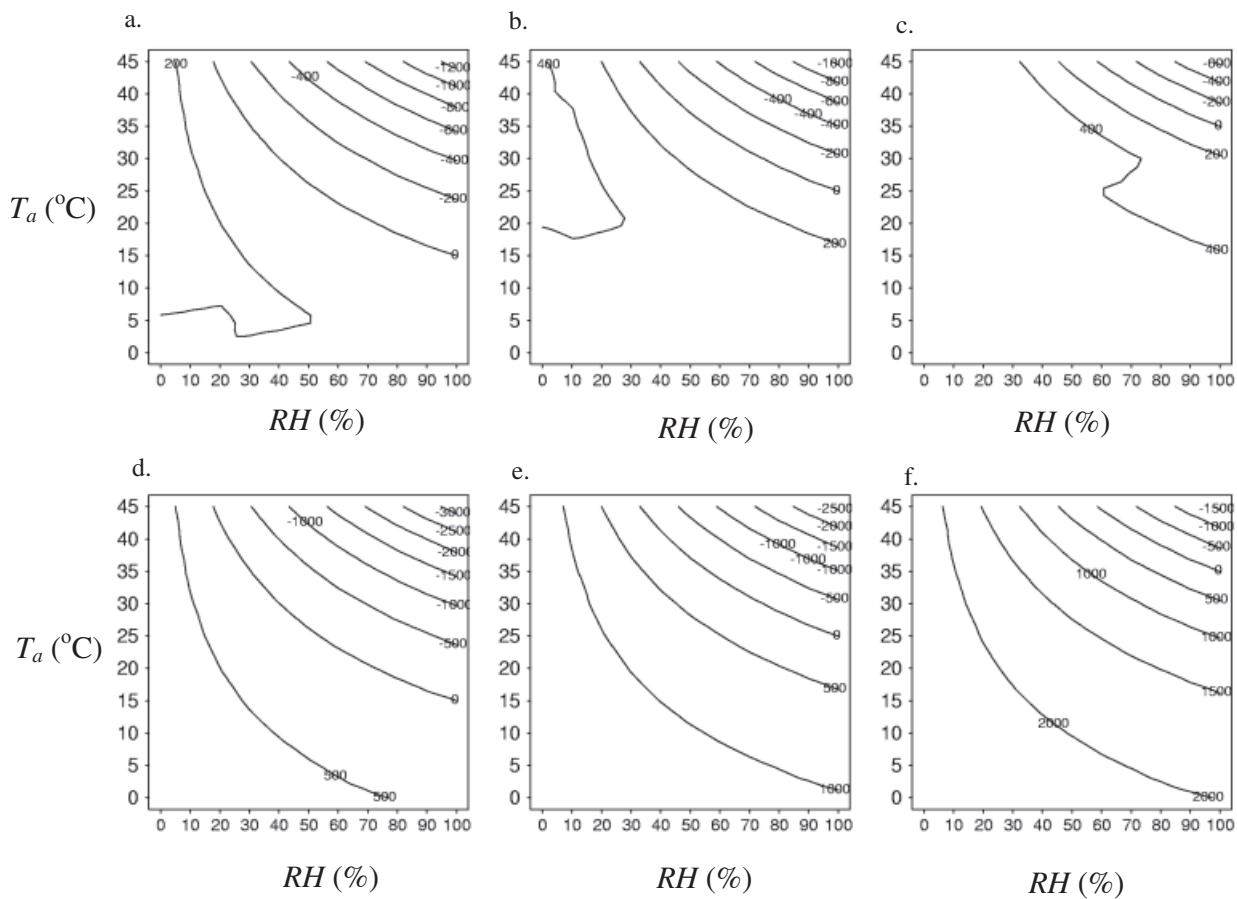


**Figure 12.** (a) Evaporation rates ( $W m^{-2}$ ) for various  $T_a$  and RH,  $U=2 m s^{-1}$ , and  $T_{c0}=15^{\circ}C$  at the time of placement; (b) as (a), but for  $T_{c0}=25^{\circ}C$ ; (c) as (a), but for  $T_{c0}=35^{\circ}C$ ; (d) as (a), but for  $U=5 m s^{-1}$ ; (e) as (a), but for  $T_{c0}=15^{\circ}C$  and  $U=5 m s^{-1}$ ; (f) as (a), but for  $T_{c0}=25^{\circ}C$  and  $U=5 m s^{-1}$ ; (g) as (a), but for  $T_{c0}=35^{\circ}C$  and  $U=5 m s^{-1}$ .

concrete temperatures and at low wind speeds and cloud cover fractions. Predicted concrete temperatures were linearly related to air temperature and humidity, cloud cover fraction, spray water volume, initial concrete temperature, and initial drop temperature. The concrete temperatures were non-linearly related to wind speed and most sensitive to wind speeds less than  $2 m s^{-1}$ .

3. The spray volume affected concrete temperatures most when wind speeds were less than  $2 m s^{-1}$  because at lower wind speeds, heat removed by runoff water was generally larger than that by evaporation. Concrete temperatures were most sensitive to the initial concrete temperature at low air temperatures, humidities and wind speeds.
4. Radiation dominated the top surface energy balances, but all terms were significant and varied depending on concrete, atmospheric and construction conditions. Most heat loss through the top surface was through evaporation and runoff water, with evaporation dominating when wind speeds were  $> 2 m s^{-1}$ .
5. Peak concrete temperature gradients were found near the top surface and the steel support beam tops around the time of peak concrete temperatures and ranged from  $-2^{\circ}C cm^{-1}$  to  $1^{\circ}C cm^{-1}$ . The rule-of-thumb critical top to bottom concrete tem-

perature difference of  $20^{\circ}C$ , above which the concrete may crack, may be exceeded when the initial concrete temperature is greater than  $20^{\circ}C$  and the afternoon air temperature is less than  $35^{\circ}C$ .

6. To achieve the lowest concrete temperatures and temperature gradients, the time of the pour should be during the late afternoon or evening (based on an eight-hour set delay due to retarders) and the initial concrete temperature should be kept at or below  $25^{\circ}C$ , especially when wind speeds are  $< 2 m s^{-1}$ . Morning pours result in the highest concrete temperatures and temperature gradient magnitudes.
7. Concrete temperatures in July at Tampa and Phoenix (which on average has higher air temperatures and lower humidities than Tampa in July) were found to be similar. The effect of the higher air temperatures on concrete temperatures at Phoenix was offset by greater evaporation rates. Such compensation reiterates the need to include all important boundary forcings in models of curing concrete.
8. Generally, evaporation rates increased for decreasing air temperatures and humidities and increasing wind speeds and surface concrete temperatures. For wind speeds  $< 2 m s^{-1}$ , the evaporation rate will likely remain  $< 830 W m^{-2}$  (the NYSDOT critical

rate) for all surface concrete temperatures and air temperatures and humidities. When heat is removed from the concrete by evaporation, the evaporation rate increased by a factor of 2–2.5 for an increase in surface concrete temperatures of 10 °C. Evaporation rates determined from a nomogram were about 15–35% lower than those from our evaporation parameterisation.

9. The SLABS forecast model, which uses numerical weather prediction model forecasts as input, outputs peak temperature and temperature gradient predictions, placement-time evaporation rates, and warning messages about conditions hazardous to the concrete. Temperature predictions from the forecast model were shown to be within 2 °C of observed temperatures at the 1999 bridge showing the model's utility as an operational field model. This application of the model showed that local effects on atmospheric conditions will influence the concrete temperatures. Specifically, obstacles acting as wind breaks can be accounted for with schemes such as that suggested by Acevedo (2001).

## 4.2. Discussion

The analysis presented here shows clearly that atmospheric and construction conditions can have a significant effect on curing concrete temperatures. Note that the results are specific for NYSDOT's Class HP concrete; other concretes may have different sensitivities. The wide range of atmospheric and construction conditions that may be encountered and the lack of data relating temperature effects to stresses in Class HP concrete make it difficult to devise a detailed set of placement and curing specifications based on the results presented here. Until more information on stress development is available, the SLABS forecast model can be used by field engineers as a guide to determine the best time for placement or the best mix design or curing practices to implement.

The SLABS forecast model has been shown to be an efficient and accurate tool with which to predict concrete temperatures based on the data we collected at four bridge decks. While our observational datasets are the most extensive ever taken for bridge decks to our knowledge, the model can only be improved and its performance further evaluated with the collection of more observational data.

To make the model more useful, information about the effect of various doses of retarders on hydration rates and set delay must be determined. Experience of the field engineer or concrete plant personnel aids the determination of the dosage rate to give a certain set delay. However, the lack of information on retarder/hydration effects casts some uncertainty on

the ability of the forecast model to provide accurate temperature predictions.

Our analysis suggests that late afternoon or early evening is generally the best time to pour concrete, based on the criteria of keeping the concrete temperatures and temperature gradients as low as possible. However, the concrete plants, construction companies and their employees may not be willing to adjust their normal operating schedules to facilitate late afternoon pours. Pouring late in the day may require the use of artificial lighting, another expense for the companies. There is also the risk that if some part of the placement and finishing operation goes wrong, the necessary part or personnel may not be available to resolve the problem, perhaps ruining the placement.

Higher binder hydration fractions near the bridge top surface, due to its proximity to the spray water source, imply that there is a vertical gradient in strength. Such a gradient may be important to the concrete's long-term durability as certain concrete sections may be affected differently by, for example, freeze-thaw cycles, the result being increased stresses within the concrete. Lower hydration fractions near the bottom of the deck could be mitigated by the addition of water-saturated lightweight aggregate to the concrete mix, perhaps reducing early thermal cracking (D. Bentz 2001, personal communication). More research on this topic is needed.

The SLABS forecast model can be adapted to predict road temperatures and conditions. We have validated the SLABS model boundary conditions with field measurements and flux estimates. Surface flux predictions of existing road models have not been evaluated. One reason for the lack of validation of the radiation flux, the dominant term of the energy balance, is that radiation measurements are rarely, if ever, taken at road weather stations. Such measurements should be made not only for the validation procedure, but also to identify microclimates. With weather model forecasts and information from the planned 400 roadside weather stations in New York State, the SLABS model adapted to the road environment can be used by NYSDOT road maintenance personnel to determine when and where to use de-icing chemicals and how much to apply, perhaps saving millions of dollars each year by reducing the amount of chemicals used and by reducing the number of personnel hours. The reduction in chemicals will decrease the damage to ecosystems along roads and better road conditions will save lives.

## Acknowledgements

We gratefully acknowledge the partial funding support from the New York State Department of Transportation's Research and Development Bureau and the Atmospheric Sciences Research Center at the

University at Albany, State University of New York. We thank Dale Bentz of the Building and Fire Research Laboratory at the National Institute of Standards and Technology in Gaithersburg, Maryland for many valuable discussions and suggestions about the cement and concrete science portion of this work. We also thank two anonymous reviewers for their comments and suggestions which have improved this paper.

## References

- Acevedo, O. (2001) Effects of temporal and spatial transitions on surface atmosphere exchanges. Ph.D. dissertation, University at Albany, State University of New York, 204 pp.
- ACI (1991) Hot weather concreting. *ACI Materials Journal* 4: 417–436.
- Bentz, D. P. (2002) Influence of curing conditions on water loss and hydration in cement pastes with and without fly-ash substitution. NISTIR 6886, 15 pp. [Available from the National Institute of Standards and Technology, 100 Bureau Drive Stop 8615, Gaithersburg, MD, 20899.]
- Bentz, D. P. & Garboczi, E. J. (1991) Percolation of phases in a three-dimensional cement paste microstructure model. *Cem. Concr. Res.* 21: 325–344.
- Bentz, D. P. & Hansen, K. K. (2000) Preliminary observations of water movement in cement pastes during curing using X-ray absorption. *Cem. Concr. Res.* 30: 1157–1168.
- Bogue, R. H. (1955) *Chemistry of Portland Cement*. Reinhold, 793 pp.
- Brutsaert, W. (1975) On a derivable formula for longwave radiation from clear skies. *Water Resour. Res.* 11: 742–744.
- Bureau of Reclamation (1988) *Concrete Manual*. US Department of the Interior, 627 pp.
- Chen, D., Gustavsson, T. & Bogren, J. (1999) The applicability of similarity theory to a road surface. *Meteorol. Appl.* 6: 81–88.
- Crevier, L.-P. & Delage, Y. (2001) METRo: a new model for road-condition forecasting in Canada. *J. Appl. Meteorol.* 40: 2026–2037.
- Emborg, M. (1990) Thermal stresses in concrete structures at early ages. Ph.D. dissertation, Luleå University of Technology, 286 pp.
- FitzGibbon, M. E. (1976a) Large pours for reinforced concrete structures. *Concrete* 10 (3): 41.
- FitzGibbon, M. E. (1976b) Large pours: 2. Heat generation and control. *Concrete*, 10 (12): 33–35.
- Freedman, J. M., Fitzjarrald, D. R., Moore, K. E. & Sakai, R. K. (2001) Boundary layer clouds and vegetation-atmosphere feedbacks. *J. Climate* 14: 180–197.
- Fujita, T. T. & Wakimoto, R. M. (1982) Effects of miso- and mesoscale obstructions on PAM winds obtained during project NIMROD. *J. Appl. Meteorol.* 21: 840–858.
- Gopalan, M. K. & Haque, M. N. (1987) Effect of curing regime on the properties of fly-ash concrete. *ACI Materials Journal* 84 (1): 14–19.
- Hjorth, L. (1982) Microsilica in concrete. *Nordic Concrete Res. No. 1 Paper 9*, Aalborg Portland, Denmark, 18 pp.
- Incropera, F. P. & DeWitt, D. P. (1996) *Introduction to Heat Transfer*, John Wiley & Sons, 801 pp.
- Jacks, E., Bower, J. B., Dagostaro, V. J., Dallavalle, J. P., Erickson, M. C. & Su, J. C. (1990) New NGM-based MOS guidance for maximum/minimum temperature, probability of precipitation, cloud amount, and surface wind. *Wea. Forecasting* 5: 128–138.
- Jacobs, A. (1997) KALCORR: a Kalman-correction model for real-time road surface temperature forecasting. KNMI Report TR-198, 23 pp. [available from Applications and Modeling Division, KNMI, Netherlands.]
- Kondo, J. & Ishida, S. (1997) Sensible heat flux from the Earth's surface under natural convection conditions. *J. Atmos. Sci.* 54: 498–509.
- Mangold, M. & Springenschmid, R. (1994) Why are temperature-related criteria so unreliable for predicting thermal cracking at early ages? In: R. Springenschmid, ed., *Thermal Cracking in Concrete at Early Ages*, Rilem Proceedings Series, Spon Press, 361–368.
- MNDOT (cited 2002) [available online at: [www.mrr.dot.state.mn.us/pavement/concrete/concrete.asp](http://www.mrr.dot.state.mn.us/pavement/concrete/concrete.asp).]
- Neville, A. M. (1996) *Properties of Concrete*. Wiley & Sons, 844 pp.
- NYSDOT (1998) Bridge deck construction specification improvements-implementation of recommendations by the Bridge Deck Task Force. NYSDOT Rep. EI 98-037, 13 pp. [available from New York State Department of Transportation Structures Division, 1220 Washington Ave., Building 5, 6th floor, W. Averell Harriman State Office Building Campus, Albany, NY, 12232-0600.]
- NYSDOT (1999) Specification revisions – Class HP concrete for substructures and structural slabs. NYSDOT Rep. EI 99-002, 22 pp. [available from New York State Department of Transportation Structures Division, 1220 Washington Ave., Building 5, 6th floor, W. Averell Harriman State Office Building Campus, Albany, NY, 12232-0600.]
- Papadakis, V. G., Fardis, M. N. & Vayenas, C. G. (1992) Hydration and carbonation of pozzolanic cements. *ACI Materials Journal* 89 (2): 119–130.
- Pommersheim, J. M. & Clifton, J. R. (1991) Models of transport processes in concrete. NISTIR 4405, 92 pp. [available from the National Institute of Standards and Technology, 100 Bureau Drive Stop 8615, Gaithersburg, MD 20899.]
- Powers, T. C. (1958) Structure and physical properties of hardened Portland cement paste. *J. Amer. Ceramic Soc.* 41: 1–6.
- Powers, T.C. & Brownyard, T. L. (1946–7) Studies of physical properties of hardened Portland cement paste (nine parts), *J. Amer. Concr. Inst.* 43.
- Prata, A. J. (1996) A new long-wave formula for estimating downward clear-sky radiation at the surface. *Q. J. R. Meteorol. Soc.* 122: 1127–1151.
- Press, W. H., Teukolsky, S. A., Vetterling, W. T. & Flannery, B. P. (1992) *Numerical Recipes in FORTRAN: The Art of Scientific Computing*. Cambridge University Press, 966 pp.
- Pruppacher, H. R. & Klett, J. D. (1997) *Microphysics of Clouds and Precipitation*. Kluwer Academic Publishers, 954 pp.
- Rayer, P. J. (1987) The Meteorological Office forecast road surface temperature model. *Meteorol. Mag.* 116: 180–191.
- Roelfstra, P. E., Salet, T. A. M. & Kuiks, J. E. (1994) Defining and application of stress-analysis- based temperature difference limits to prevent early-age cracking in concrete structures. In: R. Springenschmid, ed., *Thermal Cracking in Concrete at Early Ages*, Rilem Proceedings Series, Spon Press, 273–280.
- Sass, B. H. (1997) A numerical forecasting system for prediction of slippery roads. *J. Appl. Meteorol.* 36: 801–817.
- Shao, J. & Lister, P. J. (1996) An automated nowcasting

- model of road surface temperature and state for winter road maintenance. *J. Appl. Meteorol.* **35** 1352–1361.
- Stull, R. B. (1988) *An Introduction to Boundary Layer Meteorology*. Kluwer Academic Press, 666 pp.
- Taylor, H. F. W. (1997) *Cement Chemistry*. Thomas Telford Publishing, 459 pp.
- Verbeck, G. J. & Foster, C. W. (1950) The heats of hydration of the cements. *Longtime Study of Cement Performance in Concrete*. Proc. ASTM 50, 1235–1257.
- Watt, J. D. & Thorne, D. J. (1965) Composition and pozzolanic properties of pulverised fuel ashes. I. Composition of fly ashes from some British power stations and properties of their component particles. *J. Appl. Chem.* **15**: 585–594.
- Wojcik, G. S. (2001) The interaction between the atmosphere and curing concrete bridge decks. PhD. Dissertation, University at Albany, State University of New York, 328 pp.
- Wojcik, G. S. & Fitzjarrald, D. R. (2001) Energy balances of curing concrete bridge decks. *J. Appl. Meteorol.* **40** (11): 2003–2025.
- Wojcik, G. S., Plawsky, J. L. & Fitzjarrald, D. R. (2001) Development of a bimolecular expression to describe the heat generation of Class HP concrete. *Cem. Concr. Res.* **31** (12): 1847–1858.